Probing the Intrinsic Ability of Particles to Generate Reactive Oxygen Species and the Effect of Physiologically Relevant Solutes

Part 2: Laboratory Results

FINAL REPORT

Contract No. 10-314

Prepared for:

California Air Resources Board

Prepared by:

Dr. S.E. Paulson, Dr. A. Hasson and Dr. C. Anastasio

Researchers:

UCLA: Michelle Xiaobi Kuang, J. Adlin Scott, David H. Gonzalez-Martinez, Tiffany Charbouillot

CSU Fresno: Kennedy K-T Vu, James Baroi, Catalina Olea, Annabelle Lolinco, Kylie Markarian

UCD: Jessica G. Charrier, Alexander S. McFall, Nicole K. Richards-Henderson

May 2016

DISCLAIMER

The statements and conclusions in this Report are those of the contractor and not necessarily those of the California Air Resources Board. The mention of commercial products, their source, or their use in connection with material reported herein is not to be construed as actual or implied endorsement of such products.

Table of Contents

iii. List of Figures 4

iv. List of Tables 7

III. Laboratory Results 8

III.A. HOOH production from individual chemicals 8

III.B Rate of ˙OH production from individual redox-active species 16

III.C. DTT Response from Theoretical PM sample 25

III.D. Dithiothreitol (DTT) Redox-Activity of Particulate Matter from Field Campaigns 37

III.E. Hulis separation method development 42

III.E.1 Introduction 42

III.E.2. Specific Methods 44

III.E.3. Separation of hydroxy terephthalate from fulvic acid, humic acid, and biomass burning humic like substances. 44

III.G. References 50

iii. List of Figures

Figure 1. Initial rates of HOOH production from 500 nM of individual metals and quinones in a SLF with four antioxidants. Error bars represent one standard deviation of replicates (n ≥ 2). Asterisks mark rates that are statistically larger than zero ($p < 0.05$). The rate for 1,2-NQN (44 ± 4 µM/hr) is divided by 10 to fit on this scale. 8

Figure 2. Concentration-response curves of the rates of HOOH production as a function of concentration of redox-active species. Regression equations for the species are given in Table 1. 9

Figure 3. Effect of antioxidant composition on the rate of HOOH production from 250 nM Cu(II) in pH 7.3 phosphate-buffered saline. When present, the concentration of each antioxidant is constant for all experiments: Asc is 200 µM, Cit is 300 µM, and GSH and UA are each 100 µM. The final solution composition, with all four antioxidants, is our SLF condition used in all other figures. Each sample rate is corrected by a blank containing the same composition of antioxidants. 10

Figure 4. Measured initial rates of HOOH production in laboratory mixtures of quinones and/or transition metals (grey bars) compared to the calculated sum of the rates from the individual redox-active species (stacked colored bars). Error bars of the colored stacked bars are the propagated errors of the sum (all have replicate samples). The concentration of metals and quinones is constant: Cu, Fe and PQN are at 500 nM and 1,2-NQN is at 20 nM. 12

Figure 5. Impact of iron on HOOH production in laboratory solutions and suppression of HOOH production in extracts of ambient particles. Panel (a) shows the normalized HOOH production – the measured rate of HOOH formation in laboratory mixtures containing copper and/or quinones and iron divided by the expected (calculated) rate from just the copper and quinones. The rate of HOOH production in the absence of Fe is measured directly for all cases except the three diamonds marked with a bold outline, where HOOH production was calculated based on the concentration of Cu. Black lines in Panel (a) are the model fits to the data, with equations noted on the lines. Panel (b) shows the normalized HOOH production for ambient particle extracts from Fresno, California, where the expected rate was calculated using only the copper concentration. The last two panels compare the measured rates of HOOH production in ambient PM extracts with: (c) the calculated HOOH rates based on the fit to the laboratory solutions in Panel (a), and (d) the calculated rates based only on the concentrations of soluble Cu in the ambient PM extracts. 14

Figure 6. Rates of ˙OH and HOOH production from 500 nM of individual redox-active species. The error is the standard deviation of replicates (n ≥ 2). HOOH rate data are from past work (2014); Fe(II) destroys background HOOH, resulting in a slightly negative rate of HOOH production. Note that the 1,2-NQN rate of HOOH production and error bar are divided by 10 to fit on the scale. 17

Figure 7. Rates of ˙OH production as a function of concentration of individual redox-active species. Equations for the regression lines are listed in Table 2. 17

Figure 8. Rate of ˙OH production measured in a mixture (right grey bar) and calculated as the sum from individual species (left stacked bar). The difference within each pair of bars represents the synergistic ˙OH production from Fe. Errors on grey bars are the standard deviation of replicate

measurements, while errors on colored bars are the propagated error of replicate measurements for each species in the bar. 19
Figure 9. Measured versus predicted rates of ˙OH production from mixtures of Fe, Cu and/or quinones. The predicted ˙OH is calculated using equation 6 in Table 2. This equation works for mixtures of Fe and Cu (triangles) and mixtures of Fe and/or Cu and quinones (circles). 20
Figure 10. Suppression in the rate of HOOH formation, and corresponding enhancement in the rate of ˙OH formation, when Fe is added to a solution. The change in each HOOH rate is negative (i.e., adding Fe suppresses HOOH formation), but is plotted here as the absolute value. Each x-axis label indicates the composition of the solution and the concentration (in nM) of each metal and/or quinone. HOOH data are from past work (2014). 22
Figure 11. Contributions from individual species, and synergistic effects with Fe, towards ˙OH production for three hypothetical extracts of ambient PM using low, median, and high concentrations of particulate redox-active species reported in the literature. Data are displayed as a percentage of the total rate, with the absolute rate (R_{OH}) listed below in units of µM/hr. . 23
Figure 12. Relative contributions of redox-active species to a) DTT loss (Charrier and Anastasio 2012b), b) HOOH production (Charrier et al. 2014), and c) ˙OH production (this work) using the median particulate concentrations of ambient quinones and soluble metals reported in the literature. 24
Figure 13. DTT Response from a theoretical particle sample in units of (a) µM DTT per minute (linear scale) and (b) pmols DTT per minute per µg PM (log scale). The theoretical PM sample would produce soluble concentrations of 100 nM Cu, 150 nM Mn, 150 nM Co, and 5 nM PQN at a mass concentration of 10 µg PM per mL DTT solution. 26
Figure 14. Calculated contributions of soluble metals and quinones to the measured DTT response for eight ambient $PM_{2.5}$ samples. The PM mass concentration added to the DTT assay for each sample is given below the x-axis label. For each sample the total bar height represents the measured DTT response, and the colored components of the bar are the calculated contributions from individual chemical components, using measured component concentrations and the concentration-response curves from Charrier and Anastasio (2012). The grey portion of the bar represents the DTT response from unknown species. 27
Figure 15. Measured DTT response as a function of PM concentration added to the assay for the eight ambient $PM_{2.5}$ samples. Data are displayed in two units (a) µM DTT per minute, and (b) pmols DTT per minute per µg PM. Each color represents an individual sample (Table 3). 28
Figure 16. Summary of results from sample C12, including the measured soluble Cu concentration (right Y-axis), and measured DTT rate and calculated DTT rate from Cu (left Y-axis) for (a) the raw measurement, and (b) the mass-normalized measurement. 29
Figure 17. Measured rate of DTT response (blue circles) and the corrected rate determined at 10 µg PM per mL using the "interpolation" method (black x) for each PM sample. The black line represents the linear regression fit to the measured DTT response, which was used to interpolate (or extrapolate) the DTT response to a PM concentration of 10 µg per mL. The orange line in panel (g) represents the calculated DTT response based on the chemical composition of the sample measured at 65.9 µg PM per mL DTT solution. 32
Figure 18. Corrected mass-normalized DTT response using the "calculated" method as a function of starting PM mass concentration. 33

Figure 19. Corrected mass-normalized DTT rate for each sample determined using two methods, compared to the measured DTT rate. 35
Figure 24. Water-soluble BBHULIS extracted from a nighttime sample (Jan. 22) collected in winter in Fresno, in SLF, with a mass concentration of 40.5μg/m^3. 46
Figure 25. Original aqueous extract of biomass burning aerosol sample without separation (upper left panel); separation of HTA from HULIS using 90% methanol as eluent system, 1:3.3 dilution (upper right panel) and separation of HTA from HULIS using 70% phosphate buffer and 30% methanol as eluent system, 1:6 dilution (lower panel). 48
Figure 26. Separation of HTA (800nM) from 20μg/mL (upper left panel), 40μg/mL (upper right panel) and 60μg/mL of HA (lower panel) using 70% phosphate buffer at pH4 and 30% methanol as eluent. 49

iv. List of Tables

Table 1. Empirical regression equations for HOOH concentration-response curves. 9
Table 2. Regression equations for the rate of ˙OH production as a function of concentration of individual and mixed redox-active species. 18
Table 3. Summary of the subset of Claremont and Fresno samples used for the variable mass analysis in this chapter. 27

III. Laboratory Results

III.A. HOOH production from individual chemicals

As a first step in identifying the components in PM that can produce HOOH, we started by screening HOOH formation from individual chemicals at a concentration of 500 nM in the SLF. This is a reasonable concentration for Fe and Cu, but is over an order of magnitude higher than expected for the quinones. We started with this relatively high concentration in order to identify any compound that can produce HOOH under our reaction conditions.

Of the 10 transition metals tested, only Cu(II) produces significant HOOH under our SLF conditions, while Fe(II) destroys background HOOH, resulting in a slightly negative rate of HOOH production (Figure 4). Pb produces HOOH at a rate statistically different than the blank, though extremely slowly. The other seven metals – Mn, Co, V, Ni, Zn, Cd, Cr – do not produce HOOH, though there is some evidence that V can destroy HOOH. Of the four quinones tested, three produce HOOH – phenanthraquinone (PQN), 1,4-naphthoquinone (1,4-NQN) and 1,2-naphthoquinone (1,2-NQN) – but benzoquinone (BQN) does not. Previous measurements of HOOH production from 12 quinones in a pH 7.4 extract solution containing 100 µM dithiothreitol (DTT) as a reductant also found that the same three quinones produce HOOH, while the nine other quinones did not (Chung et al. 2006). At 500 nM, 1,2-NQN produces 16 - 33 times more HOOH than an equal concentration of Cu(II), PQN, or 1,4-NQN (Figure 1).

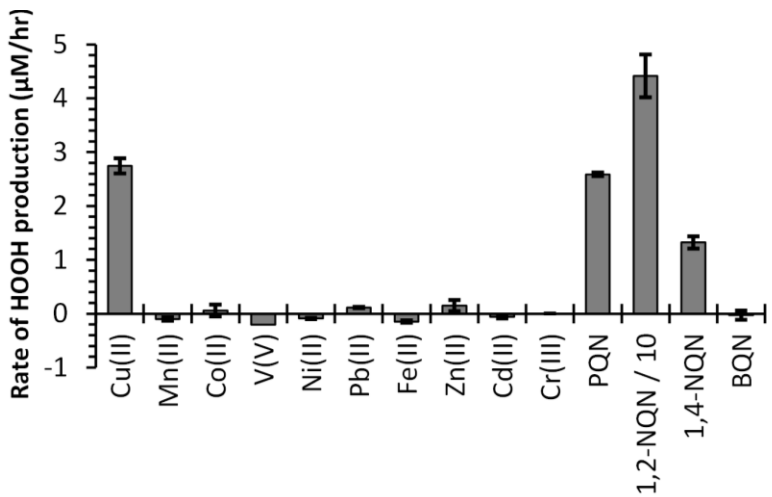

Figure 1. Initial rates of HOOH production from 500 nM of individual metals and quinones in a SLF with four antioxidants. Error bars represent one standard deviation of replicates (n ≥ 2). Asterisks mark rates that are statistically larger than zero (*p* < 0.05). The rate for 1,2-NQN (44 ± 4 µM/hr) is divided by 10 to fit on this scale.

HOOH concentration-response curves

To quantify HOOH production from Cu and quinones at concentrations relevant to ambient PM, we next measured HOOH rates as a function of concentration for the four active compounds. As shown in Figure 2, the concentration responses of all three quinones are linear, with slopes (Table 1) that indicate their relative ability to produce HOOH. The relative reactivities of the quinones in our SLF are 23 : 2 : 1, i.e., 1,2-NQN >> PQN > 1,4-NQN. A previous study of HOOH production from quinones in pH 7.4 phosphate buffer with 100 µM DTT as a reductant show a different relative reactivity, PQN > 1,4-NQN = 1,2-NQN (Chung et al. 2006).

This difference is likely due to the difference in antioxidant composition and reductant. Our SLF uses ascorbate (Asc) as the reductant and contains three other antioxidants, while Chung et al. (2006) used a PBS that contains only DTT. The reductive potential of DTT (-0.33 V) (Cleland 1964) is much stronger than Asc (+0.105) (Merkofer et al. 2006), and our antioxidant composition affects HOOH production (see next section). We have previously shown that PQN is much more active in the DTT assay relative to Cu than in our SLF (Charrier and Anastasio 2012c). When both species are at a concentration of 500 nM, PQN produces the same rate of HOOH production as Cu (Figure 2), while at the same concentration PQN causes 9 times more DTT loss than Cu (Charrier and Anastasio 2012c).

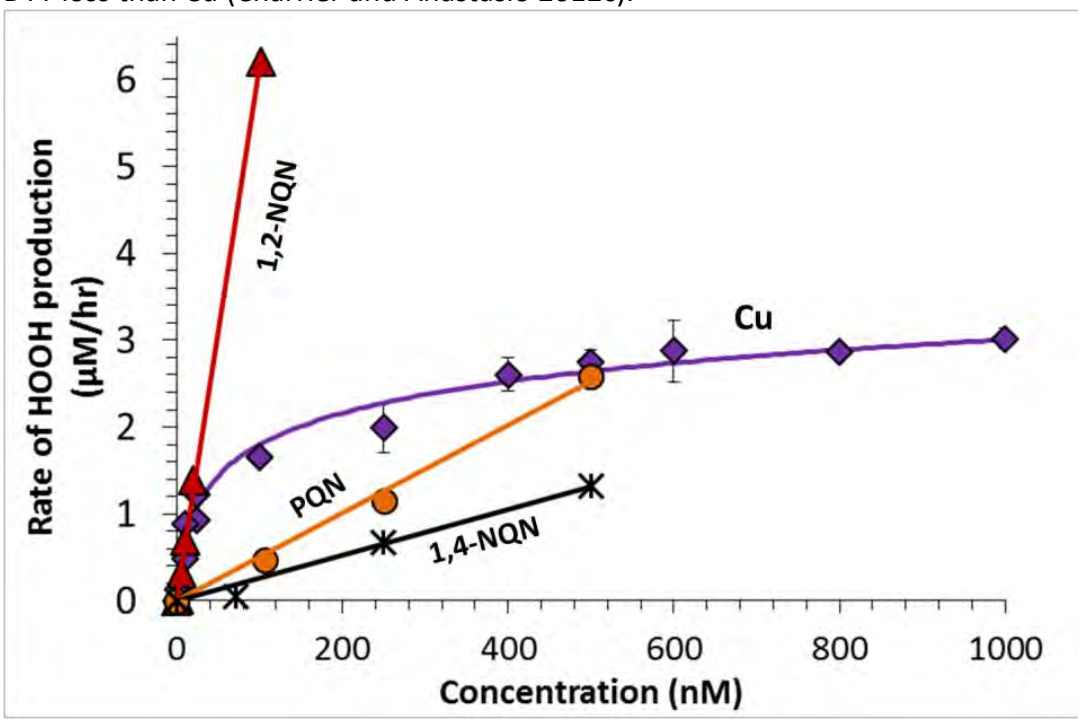

Figure 2. Concentration-response curves of the rates of HOOH production as a function of concentration of redox-active species. Regression equations for the species are given in Table 1.

Table 1. Empirical regression equations for HOOH concentration-response curves.

Compound	Equation [a]	R^2	Concentration Range (nM)	Number of Concentrations Tested
Cu	$Y = 0.524 * \ln(X) - 0.615$	0.98	3.4 - 1,000 [b]	11
PQN	$Y = 0.0050 * X$	0.99	0 - 500	4
1,2-NQN	$Y = 0.061 * X$	0.998	0 - 100	6
1,4-NQN	$Y = 0.0026 * X$	0.98	0 - 500	4

[a] *Y* is the initial rate of HOOH production (µM/hr) and *X* is the concentration of chemical species (nM).

[b] HOOH production from Cu goes to zero at 3.4 nM; therefore, HOOH production should be assumed to be zero at copper concentrations below 3.4 nM. Rates at lower Cu concentrations are indistinguishable from the blank in our experiments.

Unlike the quinones, Cu shows a non-linear concentration response with a fast initial increase in HOOH production that begins to level off around 200 nM Cu (Figure 2). We believe this results from the loss of Asc over time, which causes Asc to become the limiting reactant. As we will describe below (Figure 3) Asc acts as a reductant and is necessary for formation of both HOOH and ˙OH in our SLF. Once Asc becomes limiting, addition of more Cu causes only small increases in the rate of HOOH production. A result of the non-linear behavior is that the relative reactivity of Cu compared to quinones changes depending on the concentrations of each compound in solution. We found a similarly non-linear concentration-response curve for Cu in the DTT assay, which measures the oxidative potential of PM by monitoring the oxidation of DTT over time (Charrier and Anastasio 2012c). Thus, this result is not limited to the SLF experimental conditions in the HOOH assay. Previous laboratory studies measured the concentration-response curve for HOOH production from Cu(II) in a SLF containing only 50 µM Asc was linear through 400 nM Cu but began to plateau at 600 nM Cu, the maximum concentration tested (Shen and Anastasio 2012). This indicates that the antioxidant mixture in the SLF alters the concentration-response behavior. One implication of the non-linear Cu curve in Figure 2 is that after 200 nM, large increases in Cu concentration cause only small increases in the rate of HOOH production. At low concentrations (< 50 nM), Cu and 1,2-NQN have very similar reactivities, while at higher concentrations 1,2-NQN is much more reactive than Cu. However, this is tempered by the differences in particle concentrations of these two species: For typical ambient conditions, the concentration of Cu in a SLF extract of PM will be approximately 100 – 1000 times larger than that of 1,2-NQN. Therefore, Cu should dominate HOOH production from ambient PM. While filter-based quinone measurements may have both negative (volatilization) and positive (formation from ozone) artifacts (Chung et al. 2006), the magnitudes of these artifacts are unlikely to be large enough to make 1,2-NQN more significant than Cu as a source of HOOH for typical ambient PM.

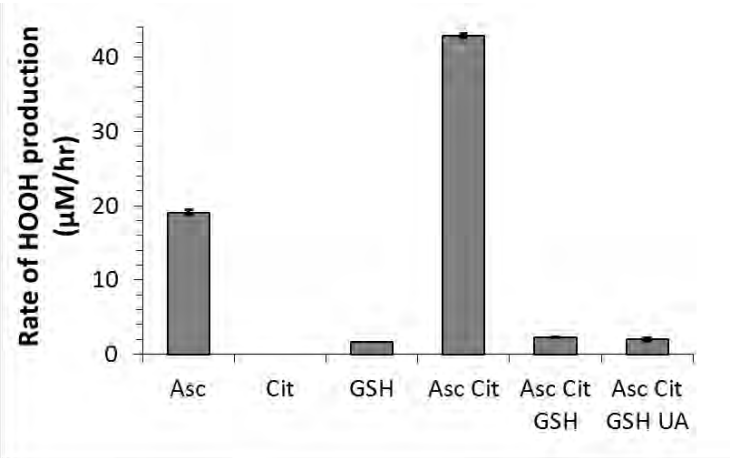

Figure 3. Effect of antioxidant composition on the rate of HOOH production from 250 nM Cu(II) in pH 7.3 phosphate-buffered saline. When present, the concentration of each antioxidant is constant for all experiments: Asc is 200 µM, Cit is 300 µM, and GSH and UA are each 100 µM. The final solution composition, with all four antioxidants, is our SLF condition used in all other figures. Each sample rate is corrected by a blank containing the same composition of antioxidants.

Effect of antioxidants on HOOH production

Our SLF includes four antioxidants: ascorbate (Asc), citrate (Cit), glutathione (GSH) and urate (UA). In previous work using the same SLF we found that the antioxidant composition has a significant effect on $^{\cdot}OH$ production from transition metals (Charrier and Anastasio 2011). Because HOOH is a precursor for $^{\cdot}OH$ we expect that these antioxidants also affect HOOH production. We test different mixtures of antioxidants to better characterize our assay, however, the base case is a SLF with all four antioxidants. This base case is used for all experiments excluding Figure 3.

As expected, HOOH production by 250 nM Cu is affected by the antioxidant composition (Figure 3). Cu produces HOOH in the presence of Asc, and to a much smaller extent in the presence of GSH only, but not in the presence of Cit only. Asc acts as the reductant in our system, cycling transition metals from their oxidized to reduced forms and thereby allowing oxidant production from Cu(II) via pathways such as:

$$Asc^{ox} + Cu(II) \rightarrow Cu(I) + Asc^{red} \quad \text{(Rxn. 1)}$$
$$Cu(I) + O_2 \rightarrow {}^{\cdot}O_2^{-} + Cu(II) \quad \text{(Rxn. 2)}$$
$$Cu(I) + {}^{\cdot}O_2^{-} \rightarrow HOOH + Cu(II) \quad \text{(Rxn. 3)}$$
$$Cu(I) + HOOH \rightarrow {}^{\cdot}OH + {}^{-}OH \quad \text{(Rxn. 4)}$$

Although Cu with GSH produces HOOH (Figure 3), this mixture does not form $^{\cdot}OH$ (Charrier and Anastasio 2011). Compared to Asc only, the combination of Asc and Cit doubles the rate of HOOH production, to 43 µM/hr for 250 nM Cu(II). Under the conditions with Asc and Cit as the only antioxidants, 100% of Cu(II) is bound to Cit (Charrier and Anastasio 2011). Thus the Cu(II)-citrate complex is apparently more reactive than free Cu(II), which is the dominant Cu form in the Asc-only condition (Charrier and Anastasio 2011). If we add GSH to the Asc Cit mixture, the production of HOOH plummets by a factor of 20, to 2.2 µM/hr, which is similar to the HOOH production rate from our SLF case with all four antioxidants. Thus, UA does not affect HOOH production from Cu in the presence of the other antioxidants. Overall, HOOH production in our mixture with all four antioxidants is substantially reduced because of GSH, likely because GSH binds to Cu and reduces its reactivity. A similar suppression by GSH was observed for $^{\cdot}OH$ production from Cu(II) in the same SLF (Charrier and Anastasio 2011), and also in other studies of $^{\cdot}OH$ from Cu (Hanna and Mason 1992; Maestre et al. 1992). MINTEQ speciation modeling of a similar SLF with the same four antioxidants shows that GSH replaces Cit as the primary ligand, and 100% of Cu(II) is bound to GSH under these conditions (Charrier and Anastasio 2011). GSH is well known as an important antioxidant *in vivo*, and may be especially important in mitigating damage from HOOH (Mulier et al. 1998). Binding and deactivating Cu may be one component of this protective effect of GSH.

We also find that the antioxidant mixture affects the ability of quinones to generate HOOH. Compared to the case of Asc only, HOOH production in the four antioxidant (SLF) mixture is lower by factors of 2 and 6 for 500 nM PQN and 20 nM 1,2-NQN, respectively. While HOOH formation from the quinones is less sensitive to antioxidant composition than is Cu, the impact on quinones is surprising and more work is necessary to confirm this result and understand its mechanism.

HOOH production from mixtures of metals and quinones

Ambient PM samples contain a complex mixture of chemical species that may produce HOOH in a more complicated mechanism than in the pure laboratory solutions measured here. For example, quinones and Cu can act synergistically to produce HOOH under some conditions: Semi-quinone radicals can reduce Cu(II) to Cu(I), producing superoxide that can react with Cu(I) to make HOOH (Li and Trush 1993; Wang et al. 2012). To examine this in our SLF, we measured HOOH production in mixtures of Cu, quinones and/or Fe (Figure 4). The grey bars in Figure 4 represent the rate of HOOH production measured from the species mixed in the same bottle, while the colored stacked bars are the sum of HOOH production measured from the individual compounds.

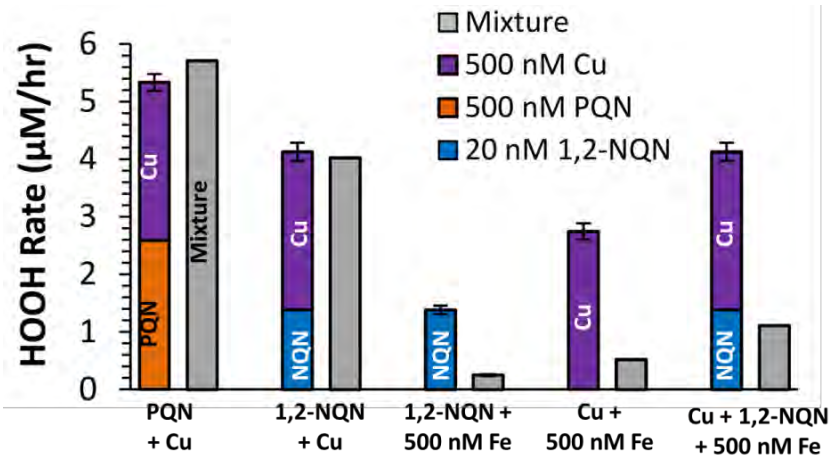

Figure 4. Measured initial rates of HOOH production in laboratory mixtures of quinones and/or transition metals (grey bars) compared to the calculated sum of the rates from the individual redox-active species (stacked colored bars). Error bars of the colored stacked bars are the propagated errors of the sum (all have replicate samples). The concentration of metals and quinones is constant: Cu, Fe and PQN are at 500 nM and 1,2-NQN is at 20 nM.

As shown by the first two sets of bars, the rate of HOOH production in a mixture of a quinone and Cu is the same as the sum of the rates of the individual species; i.e., HOOH production from Cu and either 1,2-NQN or PQN is additive (Figure 4). Thus, reactions between Cu and quinones appear to be negligible for HOOH formation in this system. This may be due to the presence of Asc, which rapidly cycles Cu(II) to Cu(I) and is present at a concentration that is 400 – 10,000 times higher than the quinones; we expect a similar Asc dominance in lung lining fluid in vivo. This likely causes most Cu(II) to react with Asc instead of a semi-quinone radical. In contrast to the additive behavior of Cu with quinones, the addition of 500 nM Fe to SLF containing Cu and/or 1,2-NQN, greatly reduces HOOH formation, to 20 – 30% of the rate measured without Fe (Figure 4). This decrease in the rate of HOOH formation might be because Fe is suppressing the formation of HOOH from Cu or quinones, or because Fe(II) is destroying HOOH and converting it to ˙OH via the Fenton reaction. We cannot deduce which mechanism is at work here, but plan to explore this in the future by looking at ˙OH production from the same mixtures. Based on these results, Fe may have an important role in suppressing HOOH generation in ambient PM extracts since ambient concentrations of Fe are high, resulting in SLF concentrations up to a few micromolar under typical sampling conditions.

Suppression of HOOH production by Fe

We further investigated the effect of Fe by quantifying HOOH production in 17 laboratory solutions containing mixtures of Fe with Cu, 1,2-NQN,1,4-NQN and/or PQN. We express the impact of Fe in Figure 5a using the "normalized HOOH production rate", which is a value between 0 and 1 calculated according to:

Normalized HOOH production = (Measured HOOH rate)/(Expected HOOH rate without Fe) (R1)

The numerator is the measured HOOH rate in the mixture (including Fe), while the denominator is the HOOH rate in the absence of Fe, which was either measured directly or determined based on the Cu and/or quinone concentrations in conjunction with the concentration-response curves in Table 1. As an example, a normalized HOOH production value of 0.7 indicates the HOOH rate in the presence of Fe is 70% of the rate in a similar solution without Fe (i.e.,. there is a 30% suppression by Fe).

Figure 5a shows that Fe has a similar effect on all of the laboratory mixtures: the normalized rate of HOOH production decreases with increasing Fe concentration between 0 and 270 nM and is relatively stable – at approximately 20% of the rate in the absence of Fe – at higher Fe concentrations. We applied the same analysis to 39 ambient samples collected in Fresno, CA during 2008 and 2009 (Bein et al. 2009). We measured both the concentration of soluble metals and the initial rate of HOOH production from these samples, but did not measure the concentration of quinones (Richards-Henderson et al. 2014). We calculate the normalized rate of HOOH production from the ambient extracts using the expected rate from soluble Cu since quinone concentrations are unknown (Figure 5b). Compared to the laboratory mixtures, Fe appears to have nearly the opposite effect on HOOH production in the ambient PM extracts: there is generally less suppression of HOOH formation as the concentration of Fe increases (Figure 5b), but the relationship is very scattered and there is no strong trend. How could higher concentrations of Fe lead to a smaller suppression of HOOH production by Fe? One possibility is that samples with higher Fe concentrations also contain higher amounts of organic ligands, which are binding to Fe and reducing its ability to reduce HOOH formation. In our laboratory solutions Cit is the dominant ligand for Fe (Charrier and Anastasio 2011) and the Fe-Cit complex clearly suppresses HOOH formation (Figure 5a). It is also possible that Cu produces HOOH less efficiently in ambient samples compared to in our laboratory solutions due to the presence of organic ligands (Figure 5b).

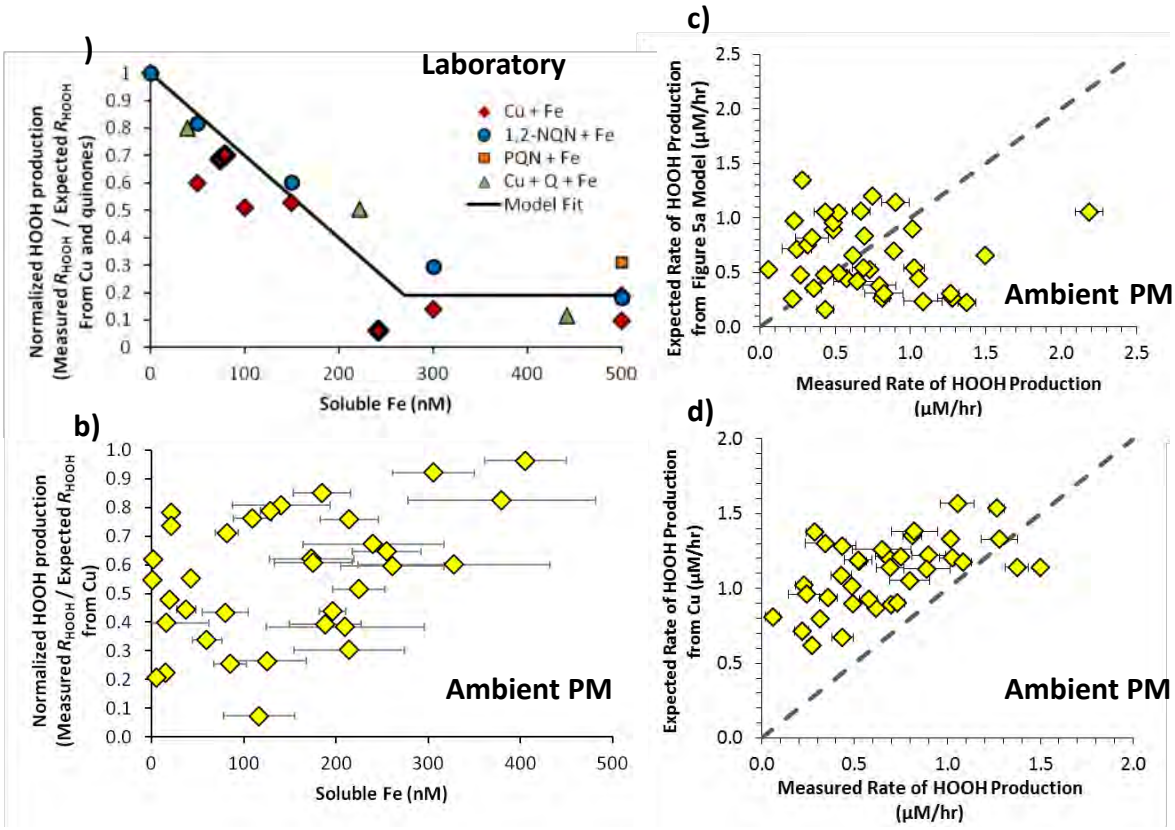

Figure 5. Impact of iron on HOOH production in laboratory solutions and suppression of HOOH production in extracts of ambient particles. Panel (a) shows the normalized HOOH production – the measured rate of HOOH formation in laboratory mixtures containing copper and/or quinones and iron divided by the expected (calculated) rate from just the copper and quinones. The rate of HOOH production in the absence of Fe is measured directly for all cases except the three diamonds marked with a bold outline, where HOOH production was calculated based on the concentration of Cu. Black lines in Panel (a) are the model fits to the data, with equations noted on the lines. Panel (b) shows the normalized HOOH production for ambient particle extracts from Fresno, California, where the expected rate was calculated using only the copper concentration. The last two panels compare the measured rates of HOOH production in ambient PM extracts with: (c) the calculated HOOH rates based on the fit to the laboratory solutions in Panel (a), and (d) the calculated rates based only on the concentrations of soluble Cu in the ambient PM extracts.

If we apply the laboratory solutions model from Figure 5a to ambient PM we can calculate the expected HOOH production based on the concentration of Cu and Fe in each sample. When we plot the measured versus expected HOOH production using this method (Figure 5c), the modeled data are clustered around the 1:1 line, but the R^2 value for this correlation is 0.01, indicating the model has no predictive ability. We obtain a much better relationship (R^2 = 0.3) when we calculate the expected rate of HOOH production based on only the concentration of soluble Cu using the Cu concentration-response curve (Figure 5), without considering

suppression by Fe (Figure 5d). In this case the expected rate of HOOH production is nearly always larger than the measured rate (i.e., points are almost all above the 1:1 line). This overestimate of hydrogen peroxide rates suggests HOOH production is suppressed in ambient PM extracts, but that this suppression is not strongly tied to the soluble Fe concentration. It is also possible that organic ligands from the particles are binding to Cu and suppressing its ability to form HOOH. If we assume that Cu controls HOOH formation in Figure 5d (i.e., if the contribution from quinones is negligible), the average (± 1σ) suppression in HOOH formation by Cu in ambient PM extracts is 44 ± 22% (median suppression = 40%; range = 3.7 to 93%. More work is needed to determine whether this suppression is due to Fe or to a reduction in Cu reactivity by organic ligands, but the chemistry of HOOH production in ambient particles is clearly complicated. However, the similarity between the measured rate of HOOH production and that predicted by Cu (Figure 5d) indicates that Cu is likely a major contributor to HOOH production.

Implications for HOOH formation from ambient PM

Because of the variable impact of Fe on HOOH production in ambient PM extracts, and the potential for particulate ligands to reduce Cu reactivity, we cannot predict the absolute rate of HOOH production based on the concentration of soluble metals in ambient PM. However, mixtures of Cu and quinones (the only species able to make HOOH based on Figure 5a) show that the rate of HOOH production from these redox-active species is additive (Figure 5d) and that Fe has a similar suppressive effect on HOOH production from both species (Figure 5a). Thus in the case that Fe is responsible for suppressing HOOH in ambient PM extracts we can still estimate the "unsuppressed" rate of HOOH production based on the reported ranges of ambient $PM_{2.5}$ quinone and soluble Cu concentrations. Under these conditions Cu produces the largest rate of HOOH production, 0.8 to 2.9 μM HOOH per hour, across the entire range of redox-active concentrations reported in the literature. Quinones, on the other hand, exhibit very low particle-phase concentrations and generally do not contribute significantly to HOOH production. At the highest ambient concentrations, 1,2-NQN can produce on the order of 0.5 μM HOOH per hour, while the rates for 1,4-NQN and PQN are in the range 0.0 – 0.05 μM/hr, which is negligible compared to production from Cu. If we consider the lowest, median, and highest concentrations of each redox-active species, Cu accounts for nearly all HOOH production (100%, 96%, and 84%, respectively), while 1,2-NQN accounts for 0%, 2%, and 14% of total HOOH for these three scenarios, while the other quinones make up the remainder. Though the total HOOH rate in ambient PM extracts will be somewhat lower than these calculated rates, these results indicate Cu will dominate HOOH production in ambient PM.

We also consider the possibility that reduced Cu reactivity (rather than reactions with Fe) accounts for the HOOH suppression we see in ambient PM extracts (Figure 5). In this case we repeat the rate calculations above but with a 44% reduction in the rate of HOOH formation by Cu, which is the average reduction needed to explain Figure 5d. In this case, Cu is still the dominant source of HOOH in PM extracts, accounting for 100%, 93%, and 75% of HOOH formation for the lowest, median, and highest concentration scenarios. Thus, even if Cu reactivity is suppressed in ambient PM, we expect soluble Cu to dominate HOOH production in most ambient PM samples.

This result agrees with other studies that have identified Cu as important for ROS generation using a variety of techniques, including the dithiothreitol (DTT) assay (Charrier and Anastasio 2012c; Ntziachristos et al. 2007), a macrophage ROS assay (Daher et al. 2012; Hu et al. 2008), and HOOH and ˙OH measurements (DiStefano et al. 2009; Shen and Anastasio 2011a; Shen et al. 2011; Shen and Anastasio 2012). These results also agree with a recent epidemiological study that found the Cu content of PM was associated with mortality in California (Ostro et al. 2007). One important source of Cu is likely traffic emissions (Hulskotte et al. 2007; Lough et al. 2005), which have been consistently linked to adverse health effects (Gasser et al. 2009; Godri et al. 2011; Hoek et al. 2002; Hoffmann et al. 2007). For example, rats instilled with particles from multiple sites showed a statistically significantly higher response for sites with higher traffic emissions and a higher concentration of Cu, but no association with the PAH content of PM (Gerlofs-Nijland et al. 2007). Taken together these diverse studies provide consistent evidence that Cu is an important component in the health effects from airborne particles.

III.B Rate of ˙OH production from individual redox-active species

Based on our previous 24-hour measurements of total ˙OH production from transition metals, Fe and Cu produce ˙OH in SLF, while the other 8 metals we tested (Cd, Co, Cr, Mn, Ni, V, Zn and Pb) cannot (Charrier and Anastasio 2011). We started this work by measuring the rate of ˙OH production from 500 nM of Fe and Cu as well as four quinones (also at 500 nM) that have not been previously tested. These quinones – phenanthraquinone (PQN), 1,4-benzoquinone (BQN), 1,2-naphthoquinone (1,2-NQN) and 1,4-naphthoquinone (1,4-NQN) – are some of the most frequently measured in atmospheric particles (Charrier and Anastasio 2012b). BQN did not produce ˙OH while the other three quinones all produced ˙OH at a rate similar to that of Fe(II) and Cu(II) (Figure 6). While it is possible that the active quinones can produce ˙OH directly in the presence of Asc (Shang et al. 2012), it is also possible that the quinones are only able to produce HOOH and that trace Fe (or Cu) converts the HOOH to ˙OH; we explore this idea further in the next section. As shown on the right-hand axis of Figure 6, Cu(II), PQN, and 1,4-NQN each produce HOOH (Charrier et al. 2014) with a rate that is 10 times higher than their respective OH formation rate. In contrast, HOOH production by 1,2-NQN (which is divided by a factor of 10 in Figure 6) is 100 times faster than the rate of ˙OH production. Thus for these redox-active species, approximately 1% (for 1,2-NQN) or 10% (for Cu, PQN and 1,4-NQN) of the HOOH produced is converted to ˙OH in the initial 4 hours. Fe(II), on the other hand, produces no measurable HOOH and, in fact, destroys background HOOH: The concentration of HOOH over time is less than the concentration at time zero, resulting in a negative rate of HOOH production (Figure 6). Since HOOH is a necessary reactant to form ˙OH, it is likely that Fe forms HOOH but that its concentration is maintained at a very low level because Fe rapidly converts HOOH into ˙OH via the Fenton reaction (Charrier et al. 2014). Though we used the reduced from of Fe (Fe^{+2}) and the oxidized form of Cu (Cu^{+2}), rapid redox cycling of the metals by Asc means the ˙OH rate should not depend on the initial metal oxidation state.

Rates of ˙OH formation as a function of species concentration

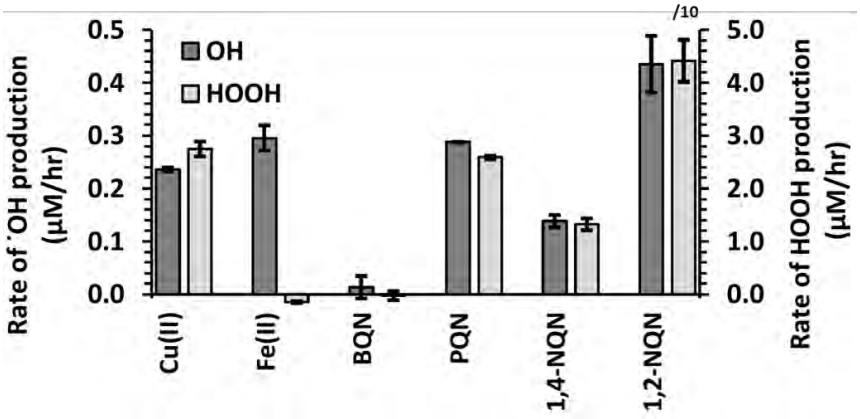

Figure 6. Rates of ˙OH and HOOH production from 500 nM of individual redox-active species. The error is the standard deviation of replicates (n ≥ 2). HOOH rate data are from past work (2014); Fe(II) destroys background HOOH, resulting in a slightly negative rate of HOOH production. Note that the 1,2-NQN rate of HOOH production and error bar are divided by 10 to fit on the scale.

Figure 7 shows the rate of ˙OH production from individual redox-active metals and quinones as a function of their concentration. For Cu, ˙OH production initially increases rapidly with Cu concentration up to approximately 25 nM, increases much more slowly after that, and nearly plateaus after approximately 200 nM Cu. 1,2-NQN and PQN show similar behavior, while 1,4-NQN exhibits a linear concentration response between 0 and 500 nM. The Fe concentration response is linear across a large Fe concentration range, but begins to plateau around 8,000 nM. We believe Cu exhibits a non-linear response because it rapidly destroys Asc, thus running out of the reductant needed to cycle Cu(II) to Cu(I). We can qualitatively identify ascorbate in our HPLC chromatograms, and observe rapid loss of the Asc peak within 2-4 hours in the presence of Cu, but not with other species. Despite this evidence, it is possible that other factors, such as the kinetics of electron transfer from Asc to the redox-active species (or from the redox-active species to O_2, $^{\bullet}O_2^{-}$, or HOOH), are controlling the concentration-response curves in Figure 7. Regardless of the mechanism, the non-linear behavior of Cu has important consequences for ˙OH production. First, at Cu concentrations larger than about 200 nM, ˙OH production is nearly constant, and an increase in Cu concentration causes only a small increase in the amount of ˙OH produced. Second, because the rate of

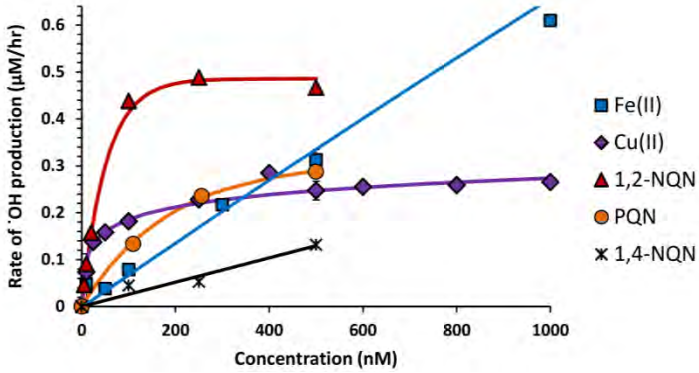

Figure 7. Rates of ˙OH production as a function of concentration of individual redox-active species. Equations for the regression lines are listed in Table 2.

Table 2. Regression equations for the rate of ˙OH production as a function of concentration of individual and mixed redox-active species.

Equation Number	Compound(s)	Regression[a]	R^2	Conc. Range (nM)[b]	Number of Data Points
Individual compounds					
Eq. 1	Cu(II)	$R_{OH} = 0.0383\times\mathrm{Ln}([Cu]) + 0.009$	0.95	0.8[c] – 10,000	14
Eq. 2	Fe(II)	$R_{OH} = (-3.13\times10^{-8})[Fe]^2 + (6.86\times10^{-4})[Fe]$	0.995	0 – 10,000	13
Eq. 3	1,2-NQN	$R_{OH} = 0.486\times(1-\exp(-0.0191*[1,2\text{-}NQN]))$	0.997	0 – 500	7
Eq. 4	1,4-NQN	$R_{OH} = (2.59\times10^{-4})\times[1,4\text{-}NQN]$	0.94	0 – 500	4
Eq. 5	PQN	$R_{OH} = 0.312\times(1-\exp(-0.0053\times[PQN]))$	0.999	0 – 500	4
Mixtures of Fe, Cu and/or quinones					
Eq. 6	Mixture	$R_{OH} = 0.198\times(R_{HOOH,Cu} + 1.56\times R_{HOOH,Q}) + 8.64E\text{-}04\times[Fe(II)]$	0.993	n/a	20
	Where:	$R_{HOOH,Cu}$ is the rate of HOOH production from Cu in µM/hr[d] $= 0.524\times\ln([Cu]) - 0.615$			
		$R_{HOOH,Q}$ is the sum of rates of HOOH from quinones in µM/hr[d] $= 0.050\times[1,2\text{-}NQN]+0.0052\times[PQN]+ 0.0024\times[1,4\text{-}NQN]$			

[a] R_{OH} is the rate of ˙OH production in µM/hr and *[X]* is the concentration of redox-active chemical species in nM .

[b] Regression equations may not be valid outside of the concentration ranges measured.

[c] The Cu(II) regression equation goes to zero at 0.8 nM of Cu(II). ˙OH values should be assumed to be zero at copper concentrations below this.

[d] The rates of HOOH production from Cu and quinones in Eq. 6 are regression equations from individual species measured previously (Charrier et al. 2014).

formation of ˙OH is not linear as a function of Cu concentration, the resulting rate will depend on how much PM is added to the assay since this determines the final Cu concentration in the extract. However, as we discuss later, the synergistic increase in ˙OH production from mixtures of Fe and Cu mitigates some of this behavior.

Comparing the rates of HOOH and ˙OH production as a function of redox-active species concentration, we find that HOOH production from Cu is 10 times larger than ˙OH production across all concentrations tested and both the HOOH and ˙OH concentration-response curves show a similar shape. This suggests that ˙OH production from Cu is tied to HOOH production. This is different than the 1,2-NQN and PQN case: these quinones show a linear increase in the rate of HOOH production with increasing quinone concentration but a weaker, non-linear response for ˙OH, which increases with quinone concentration initially then plateaus at higher concentrations. Because HOOH does not plateau, and thus does not become limiting, this result suggests that something else limits the conversion of HOOH to ˙OH at higher concentrations. This result could be explained if trace Fe is responsible for converting HOOH to ˙OH: at low quinone concentrations the rate of HOOH production is limiting ˙OH formation, but at high quinone concentrations ˙OH production is limited by the trace Fe concentration. It is unclear why the 1,4-NQN data looks different than the other quinones – in this case both HOOH

and OH formation rates are linearly dependent on quinone concentration – but it may be that the amount of HOOH produced is too little to reach a level where Fe becomes limiting.

Rates of ˙OH production in mixtures of redox-active species

While ˙OH production from individual species is an important starting point, we are more interested in the behavior of mixtures of redox-active species that mimic extracts of ambient PM. In Figure 8 we measure the rate of ˙OH production from simple mixtures of Fe, Cu and/or quinones (individual grey bars) and compare it to the sum of ˙OH production rates from individual species at the same concentrations used in the mixture (colored stacked bars). As shown in the left pair of bars, a mixture of Cu and PQN produces a rate of ˙OH that is very similar to the sum of rates from the individual species, indicating no interaction between the species. This agrees with our previous measurements of the rate of HOOH production: mixtures of Cu with either PQN or 1,2-NQN produce the same amount of HOOH as the sum of individual species (Charrier et al. 2014).

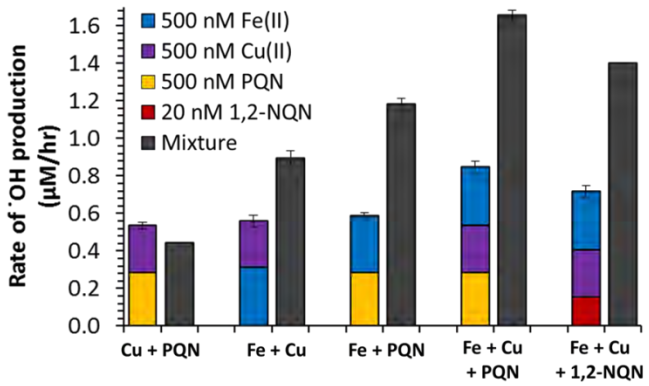

Figure 8. Rate of ˙OH production measured in a mixture (right grey bar) and calculated as the sum from individual species (left stacked bar). The difference within each pair of bars represents the synergistic ˙OH production from Fe. Errors on grey bars are the standard deviation of replicate measurements, while errors on colored bars are the propagated error of replicate measurements for each species in the bar.

We have previously shown that adding Fe to solutions containing Cu and/or quinones substantially suppresses the rate of HOOH production (Charrier et al. 2014), but that mixtures of Fe and Cu synergistically produce more ˙OH over 24 hours (Charrier and Anastasio 2011). In Figure 8, we confirm that all mixtures of Cu with Fe synergistically produce ˙OH at a rate faster than expected from the individual species. The mixture of 500 nM Fe and 500 nM Cu produces 60% more ˙OH than expected from the individual solutions, broadly consistent with our 24-hr result (Charrier and Anastasio 2011). In the case of 500 nM Fe and 500 nM PQN, the rate of ˙OH production in the mixture is twice that expected from adding the rates from the individual species, confirming that the Fe-mediated enhancement in ˙OH is not limited to Cu, but also extends to other species that make HOOH. As shown in the final two sets of bars in Figure 8, ternary mixtures of Fe, Cu and either PQN or 1,2-NQN also show synergistic behavior, with nearly a two-fold enhancement in the rate of ˙OH formation.

To further investigate this effect we measured ˙OH production from additional mixtures containing Fe, Cu and/or quinones across multiple concentration ranges. Eight of the mixtures represent the concentrations of Fe, Cu and quinones we measured in individual ambient PM

extracts (data not yet published), representing realistic PM compositions. All 20 mixtures produced ˙OH at a faster rate than predicted from the individual species, with enhancements of 19 to 131%. Based on these results, we hypothesized that synergistic ˙OH production is related to the Fenton reaction (R1). Cu and quinones form HOOH efficiently while Fe cannot efficiently form HOOH, but can convert HOOH to ˙OH. If the rate of ˙OH production from Fe individually is limited by the availability of HOOH (as indicated by complete conversion of HOOH to ˙OH in Fe solutions) then the addition of Cu and quinones will increase the available HOOH and allow Fe to convert a portion of that HOOH to ˙OH. This decreases the rate of HOOH formation as compared to Cu and quinones individually and increases the rate of ˙OH formation.

Using this hypothesis we calculated a regression equation (Eq. 6) that can predict the rate of ˙OH production based on the rates of HOOH formation by individual species and the concentration of Fe (Table 2). In this equation the rate of HOOH production is calculated from concentration-response curves of copper and quinones (Charrier et al. 2014), allowing us to predict ˙OH production in mixtures based just on the concentrations of Fe, Cu and quinones. All regression coefficients in Eq. 6 are statistically significant ($p < 0.05$) and the R^2 is 0.993. Eq. 6 accurately explains ˙OH production in our 20 mixtures for solutions that contain Fe and Cu, Fe and quinones, and mixtures of all three species. Most mixtures show excellent agreement between measured and predicted values, and only a few quinone mixtures fall just below the 1:1 line. The linear regressions of measured versus predicted ˙OH

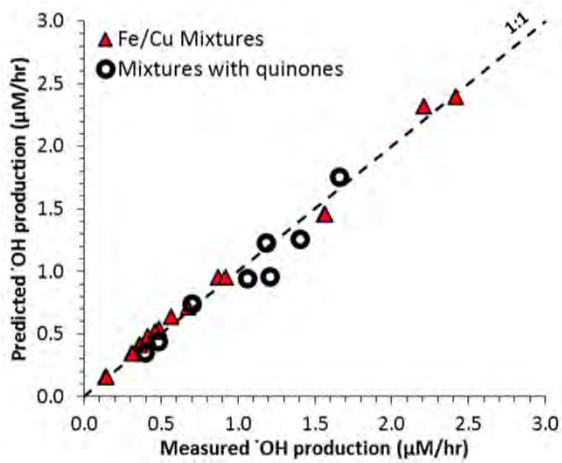

Figure 9. Measured versus predicted rates of ˙OH production from mixtures of Fe, Cu and/or quinones. The predicted ˙OH is calculated using equation 6 in Table 2. This equation works for mixtures of Fe and Cu (triangles) and mixtures of Fe and/or Cu and quinones (circles).

production is excellent both for the subset of Fe/Cu mixtures (slope ± 1 SE = 0.97 ± 0.02; R^2=0.99) and for the subset of mixtures containing metals and quinones (slope = 1.0 ± 0.1; R^2 = 0.93). In separate work we have also applied this regression to samples of ambient particulate matter and find good agreement between the measured ˙OH rate and that predicted by Eq. 6 (Richards-Henderson et al. 2015).

The fitted regression equation treats HOOH production from Cu and quinones differently, indicating a slightly different mechanism of ˙OH production. The coefficient of 1.56 before the rate of HOOH formation from quinones ($R_{HOOH,Q}$) in Eq. 6 indicates that HOOH from quinones forms ˙OH more efficiently than HOOH from Cu, suggesting a secondary mechanism in mixtures. Quinones or quinone-metal mixtures may enhance the production of ˙OH or mixtures of Fe and

Cu may suppress the formation of ˙OH. We investigate this question by comparing the impacts of Fe on the both the suppression in HOOH and the enhancement in ˙OH for a mixture with the same composition of Fe, Cu and quinones. We calculate HOOH suppression as the difference in rate for a solution containing only Cu and a solution containing the same concentration of Cu mixed with Fe. For example, the measured rate of HOOH production from 1 µM Cu minus the measured rate of HOOH production from 1 µM Cu mixed with 1 µM Fe gives the absolute decrease in HOOH production upon Fe addition. ˙OH enhancement is calculated as the rate of ˙OH production in the mixture with Fe minus the ˙OH rate in the same mixture without Fe; for example, this is the difference between the dark gray and stacked colored bars in Figure 9. If the Fenton reaction (R1) explains the impacts of Fe addition, then the suppression in HOOH would equal the enhancement in ˙OH. However, as shown in Figure 10, this is only true in two out of eight samples. In mixtures of Fe and Cu (solutions 1-6 in Figure 10) the enhancement in the ˙OH is only 20 – 34 % of the corresponding suppression in the HOOH, indicating that Fe acting via the Fenton reaction can only explain a small portion of the HOOH suppression. Adding Fe to quinone solutions (solutions 7-10 in Figure 10) results in a closer match between HOOH suppression and ˙OH enhancement, suggesting a larger role for Fenton chemistry. In solutions 7 and 9, the ˙OH rate enhancement is 50 and 58%, respectively, of the corresponding suppression in HOOH, while in solutions 8 and 10 the enhancement in the OH rate is essentially equal to the corresponding suppression in the HOOH rate. Thus, while the results of solutions 8 and 10 are consistent with Fe stoichiometrically converting HOOH to OH via R1, for the other eight mixtures it appears that the addition of Fe causes a reduction in the initial rate of HOOH production. The more efficient Fe-mediated conversion of HOOH to OH in solutions of quinones (compared to solutions containing Cu) in Figure 10 is also consistent with regression Eq. 6, which indicates that HOOH from quinones more efficiently forms ˙OH than HOOH from Cu.

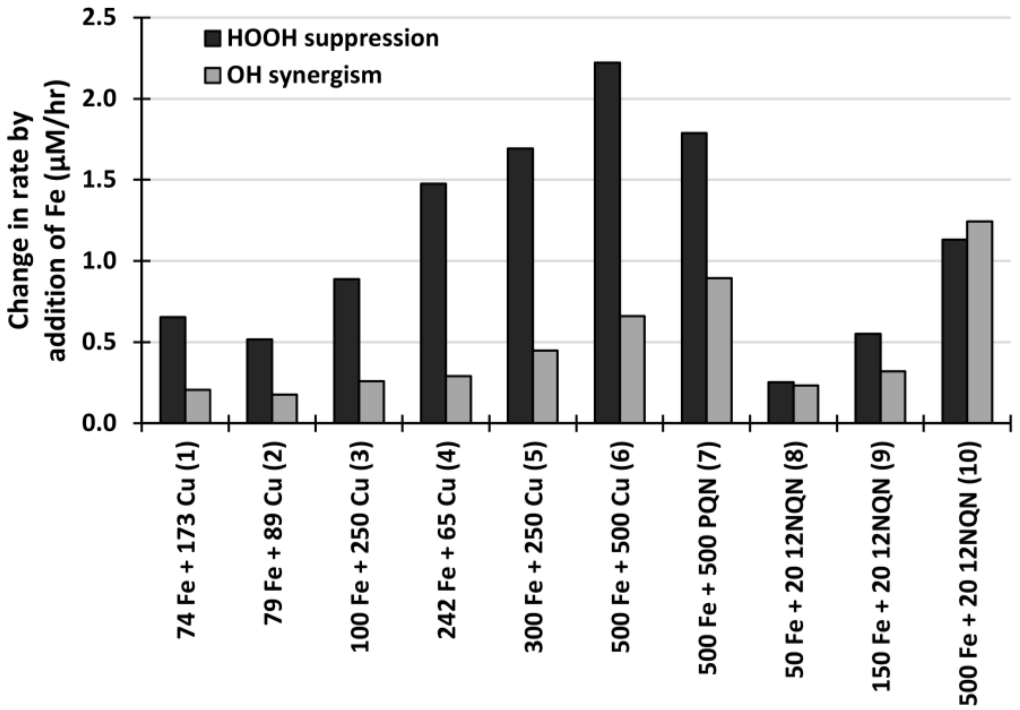

Figure 10. Suppression in the rate of HOOH formation, and corresponding enhancement in the rate of ˙OH formation, when Fe is added to a solution. The change in each HOOH rate is negative (i.e., adding Fe suppresses HOOH formation), but is plotted here as the absolute value. Each x-axis label indicates the composition of the solution and the concentration (in nM) of each metal and/or quinone. HOOH data are from past work (2014).

Implications for ˙OH production from ambient PM

We next use our concentration-response and mixture results from above, in conjunction with typical ambient concentrations of metals and quinones from the literature, to identify the relative importance of these redox-active species for ˙OH production in ambient PM extracts. While there are other redox-active species in atmospheric particles, such as humic-like substances (Lin and Yu 2011), not enough is known about their responses in the ROS assays to account for them in our calculations. We previously reported the ranges of soluble metals and particulate quinones summarized from the literature and the expected ranges of HOOH production rates from individual redox-active species (Charrier et al. 2014) . Using this same composition data we consider three cases for ˙OH: 1) "low" using the minimum reported concentration of each redox-active species, 2) "median" using the median concentration of each species, and 3) "high" using the maximum concentration of each species. While these three example cases account for the range of concentrations reported in the literature, the

actual contribution to ˙OH production for a specific particle sample will depend on its composition.

Figure 11 summarizes the relative ˙OH contribution from each species, including the synergistic contributions from Fe/Cu and Fe/quinone interactions. To determine the synergistic contributions we calculate the total rate of ˙OH production using Eq. 6, then calculate the rate for Fe and Cu using the same equation, but excluding the $HOOH_Q$ term. The difference between these two calculations gives the total ˙OH production by quinones. We then calculate the expected ˙OH production from individual quinones from Equations 3 - 5. The difference between this and the total production by quinones provides the synergistic production by quinones and Fe. Similarly we calculate the individual and synergistic contribution of Fe and Cu by subtracting the contributions from Cu and Fe individually and the total quinone contribution from ˙OH production.

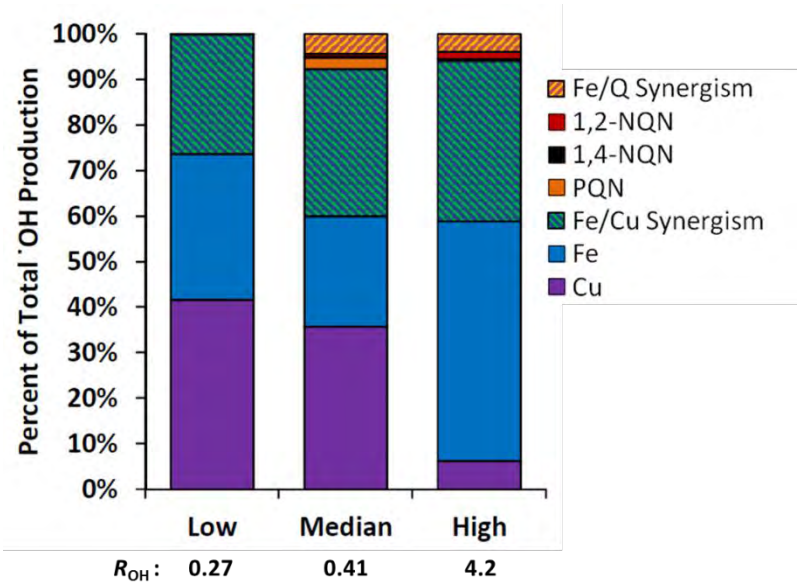

Figure 11. Contributions from individual species, and synergistic effects with Fe, towards ˙OH production for three hypothetical extracts of ambient PM using low, median, and high concentrations of particulate redox-active species reported in the literature. Data are displayed as a percentage of the total rate, with the absolute rate (R_{OH}) listed below in units of µM/hr.

Soluble Cu and Fe are most important to ˙OH production, although their relative contributions vary in the three different scenarios (Figure 11). Individually, Cu contributes 6 - 44% of total ˙OH, Fe contributes 24 – 53% and quinones contribute 0 – 3%; quinones account for a very small portion because their ambient particulate concentrations are low. Synergism between Fe and Cu is also important, accounting for 26 – 36% of ˙OH production while Fe-quinone synergy accounts for only 0.08% - 4% of total ˙OH production. Synergistic effects increase the total rate of ˙OH production by 35%, 52% and 60% in the low, median and high cases.

The relative contribution by Cu goes down as concentrations increase from the low to high case, while the relative importance of Fe goes up with increasing concentrations. This is due to the shapes of the ˙OH concentration response curves (Figure 7): Cu plateaus at very low Cu concentrations, while ˙OH production from Fe increases with increasing concentration until very high levels (around 8,000 nM). Interestingly, while the relative importance of Fe and Cu change, the relative ˙OH production from the Fe/Cu synergism stays relatively constant in these cases. Cu alone contributes just 6% of total ˙OH in the high case while Fe/Cu synergism

contributes 36%; therefore Cu is still important for total ˙OH production even though there is a plateau in the contribution from Cu individually.

Comparison with other measures of oxidative potential

In this and past work we systematically identified the responses from soluble transition metals and quinones (both individually and in mixtures) in three cell-free assays for ROS: ˙OH formation (this work), HOOH formation (Charrier et al. 2014), and dithiothreitol (DTT) loss (Charrier and Anastasio 2012b). In Figure 12 we show the relative contribution of each species to the total assay response for a hypothetical PM sample containing the median concentrations reported in the literature (Charrier and Anastasio, 2012).

For this median composition, soluble Cu accounts for a significant fraction of oxidant production in all three assays: 54% of DTT loss, 96% of HOOH production, and 36% of ˙OH production (as well as an additional 32% of ˙OH via synergy with Fe). Fe is only important in ˙OH production, but can also suppress HOOH, as we discussed above. Quinones contribute little to HOOH or ˙OH formation, but PQN accounts for a significant fraction of DTT loss. Additionally, Mn contributes a quarter to DTT loss but does not contribute to HOOH or ˙OH production.

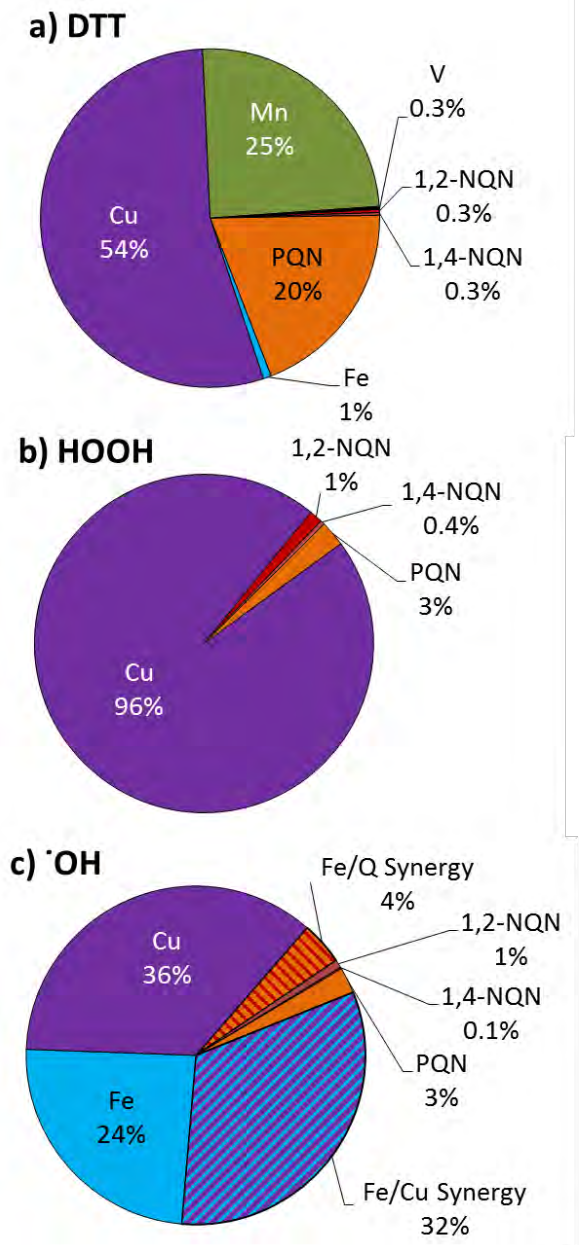

Figure 12. Relative contributions of redox-active species to a) DTT loss (Charrier and Anastasio 2012b), b) HOOH production (Charrier et al. 2014), and c) ˙OH production (this work) using the median particulate concentrations of ambient quinones and soluble metals reported in the literature.

There is one clear message from Figure 12: soluble Cu likely plays a key role in the acellular generation of ROS and oxidative stress by inhaled atmospheric particles, based on its major role in all three assays. This is consistent with previous studies of copper toxicity: (1) *in vitro* cellular assays show the Cu particles (especially nanoparticles) are remarkably toxic, likely because of ROS generation (Fahmy and Cormier 2009; Jing et al. 2015; Karlsson et al. 2013), (2) *in vivo* animal studies generally show that inhaled and instilled particulate and soluble Cu cause adverse effects (Dye et al. 2001; Pettibone et al. 2008; Rice et al. 2001), and (3) epidemiological studies reveal an association of ambient particulate Cu with adverse health effects and mortality in humans (Ostro et al. 2007; Ostro et al. 2015). Cu is known to be toxic, and is commonly used as a fungicide, pesticide, and preservative (Brun et al. 1998; Freeman and McIntyre 2008). Despite this, there is currently little regulation of airborne Cu, which is not considered a hazardous air pollutant (HAP) by the US EPA. While copper is considered a toxic air contaminant (TAC) by the California EPA, the particulate Cu chronic standard (reference exposure level or REL) set by the California Office of Environmental Health Hazard Assessment (OEHHA) is 100 $\mu g/m^3$ (OEHHA 2008). Ambient concentrations of Cu are low (0.001- 0.050 $\mu g/m^3$; (Herner et al. 2006)) but Cu dominates direct ROS production in our assays, indicating that further consideration of the potential toxicity of particulate Cu is necessary. Additionally, in all three cell-free assays, Cu exhibits a non-linear concentration-response curve, which could mask the effect of Cu when using correlation analysis or even in epidemiological studies. Finally, ROS production from Cu in cell-free assays may be confounded by high background concentrations of Cu in the salts used in the assay if Chelex treatment is not applied.

III.C. DTT Response from Theoretical PM sample

We start by examining a hypothetical particle sample to illustrate what we expect for the concentration-response curves for the overall DTT response, as well as the responses from individual DTT-active species, as a function of PM mass concentration (1 – 60 µg per mL) in the assay solution. The PM extract at 10 µg PM per mL is assumed to contain 100 nM Cu, 150 nM Mn, 150 nM Co, and 5 nM PQN. The concentration of each species is assumed to be linearly related to the PM mass concentration; that is, a doubling of PM mass concentration in the extract will double the resulting concentration of each species. While the chemical composition is linearly related to PM mass, the DTT response (in units of µM per minute) is curved for Cu and Mn, and is linear for Co and PQN (Figure 13a), a consequence of their concentration-response curves (Charrier and Anastasio 2012b). The total DTT response, which is the sum of the lines from the individual species, is then non-linear due to the contributions from Cu and Mn.

We then take the individual and total rates in Figure 13a, and divide by the PM mass concentration in the hypothetical DTT extract to determine the mass-normalized DTT response (in units of pmols DTT per minute per µg PM; Figure 13b). The mass-normalized DTT responses from PQN and Co are constant as a function of PM concentration added to the assay (since these species have linear concentration-response curves), while the mass-normalized DTT responses for Cu and Mn are not constant (since these species have non-linear concentration-response curves). Because of this, for this single hypothetical PM sample, the total DTT response varies between 30 and 445 pmols DTT per minute per µg PM and is strongly dependent on the concentration of PM added to the assay, especially at lower mass concentrations. If similar behavior occurs for ambient PM extracts, then the mass-normalized DTT rate would be highly biased, and would be essentially useless for comparing DTT responses among samples measured at different PM mass concentrations.

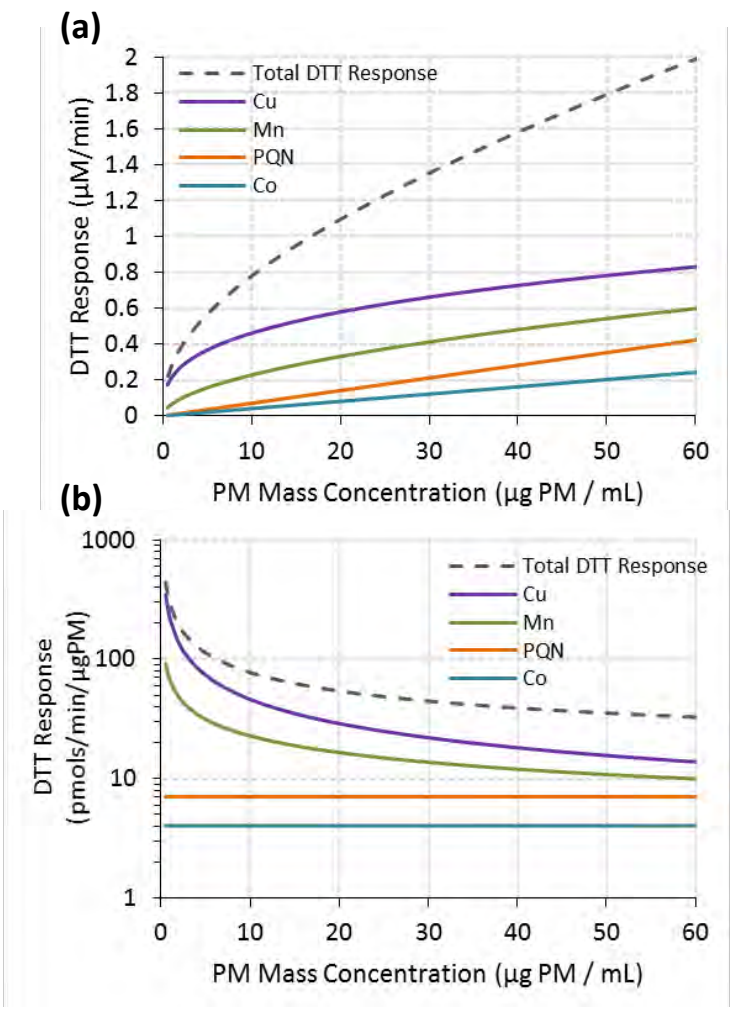

Figure 13. DTT Response from a theoretical particle sample in units of (a) µM DTT per minute (linear scale) and (b) pmols DTT per minute per µg PM (log scale). The theoretical PM sample would produce soluble concentrations of 100 nM Cu, 150 nM Mn, 150 nM Co, and 5 nM PQN at a mass concentration of 10 µg PM per mL DTT solution.

DTT Response as a Function of Ambient PM Concentration

To understand if the DTT response in ambient $PM_{2.5}$ samples behaves similarly to the theoretical PM described above, we measured the DTT response for various PM mass

concentrations for eight $PM_{2.5}$ samples collected at two locations in California. The location, date, time and range of PM

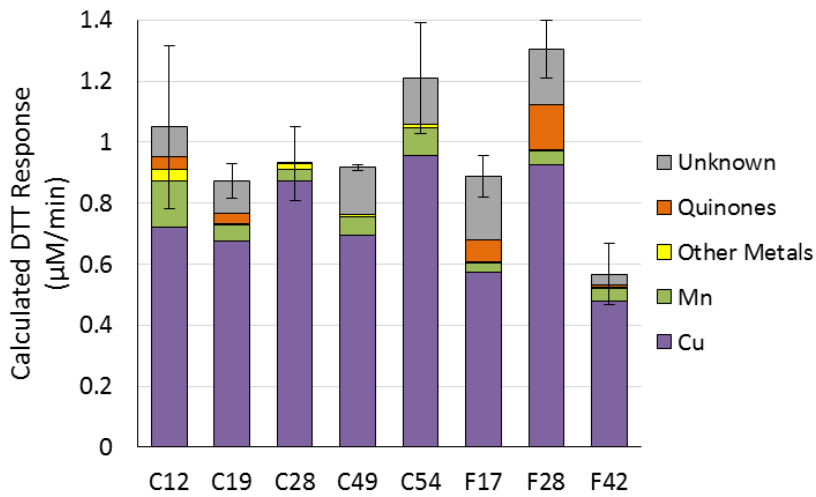

Figure 14. Calculated contributions of soluble metals and quinones to the measured DTT response for eight ambient $PM_{2.5}$ samples. The PM mass concentration added to the DTT assay for each sample is given below the x-axis label. For each sample the total bar height represents the measured DTT response, and the colored components of the bar are the calculated contributions from individual chemical components, using measured component concentrations and the concentration-response curves from Charrier and Anastasio (2012). The grey portion of the bar represents the DTT response from unknown species.

Table 3. Summary of the subset of Claremont and Fresno samples used for the variable mass analysis in this chapter.

Sample ID	Location	Date	Period	Time	Number of PM Concentrations Used in DTT assay	Range of PM Concentrations Used in DTT Assay (µg / mL)
C12	Claremont, CA	7/29 - 7/30/2012	Overnight	18:30 - 7:12	9	1.6 - 34.2
C19	Claremont, CA	8/1/2012	Morning	7:23 - 13:12	5	2.2 - 7.5
C28	Claremont, CA	8/4/2012	Morning	7:27 - 13:15	5	2.1 - 10.7
C49	Claremont, CA	8/11/2012	Morning	7:22 - 13:05	3	2.7 - 10.7
C54	Claremont, CA	8/12 - 8/13/2012	Overnight	18:17 - 7:13	4	4.0 - 24.5
F17	Fresno, CA	1/20/2013	Afternoon	13:10 - 18:00	2	15.4 - 27
F28	Fresno, CA	1/24 - 1/25/2013	Overnight	18:13 - 8:26	2	37.6 - 65.9
F42	Fresno, CA	1/30/2013	Afternoon	13:12 - 17:58	2	5.6 - 9.9

concentrations used in the DTT assay are in Table 1. We start by investigating the primary chemical species responsible for DTT loss in these samples. Based on the measured chemical composition of the PM, and the concentration-response curves measured previously (Charrier and Anastasio 2012b), we can calculate the expected DTT response from soluble metals and quinones in each sample. For Cu, we use the updated concentration-response curve discussed in the Methods section (equation 1). If the measured DTT response is larger than the sum of the calculated DTT responses from each species, then the remaining DTT response is labeled as

"unknown". Figure 14 shows the contribution of metals and quinones to total DTT response for each sample at one PM mass concentration. The DTT response from all samples is primarily attributed to Cu, while Mn and quinones (primarily PQN) make small contributions to the measured DTT response in most of these samples. Most samples also have a small contribution from "unknown" species.

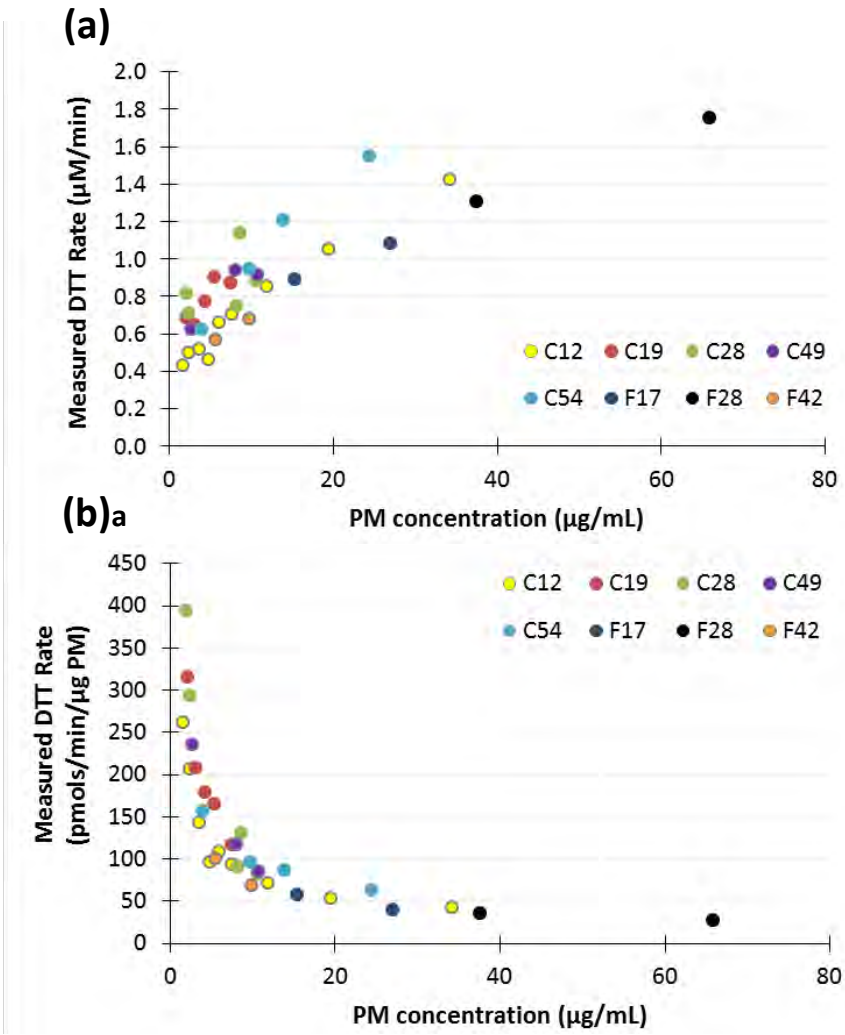

Figure 15. Measured DTT response as a function of PM concentration added to the assay for the eight ambient $PM_{2.5}$ samples. Data are displayed in two units (a) µM DTT per minute, and (b) pmols DTT per minute per µg PM. Each color represents an individual sample (Table 3).

Concentration of PM added to the vial (Figure 15b), showing similar behavior to the theoretical PM sample in Figure 13. These data unequivocally show that the mass-normalized DTT response is not constant as a function of the mass of PM added to the DTT assay, at least for samples with significant contributions to DTT activity from Cu and Mn. For a given sample, the resulting mass-normalized DTT response varies by up to a factor of 6 depending on the concentration of PM added to the assay, and this variance is primarily determined by the PM mass concentration. However, the different samples all largely follow the same curve in Figure 15b, a consequence of Cu being the dominant redox-active species in all; over the entire mass range used for the eight samples (1.6 – 66 µg/mL), the DTT rate varies by a factor of 8.

Figure 16. Summary of results from sample C12, including the measured soluble Cu concentration (right Y-axis), and measured DTT rate and calculated DTT rate from Cu (left Y-axis) for (a) the raw measurement, and (b) the mass-normalized measurement.

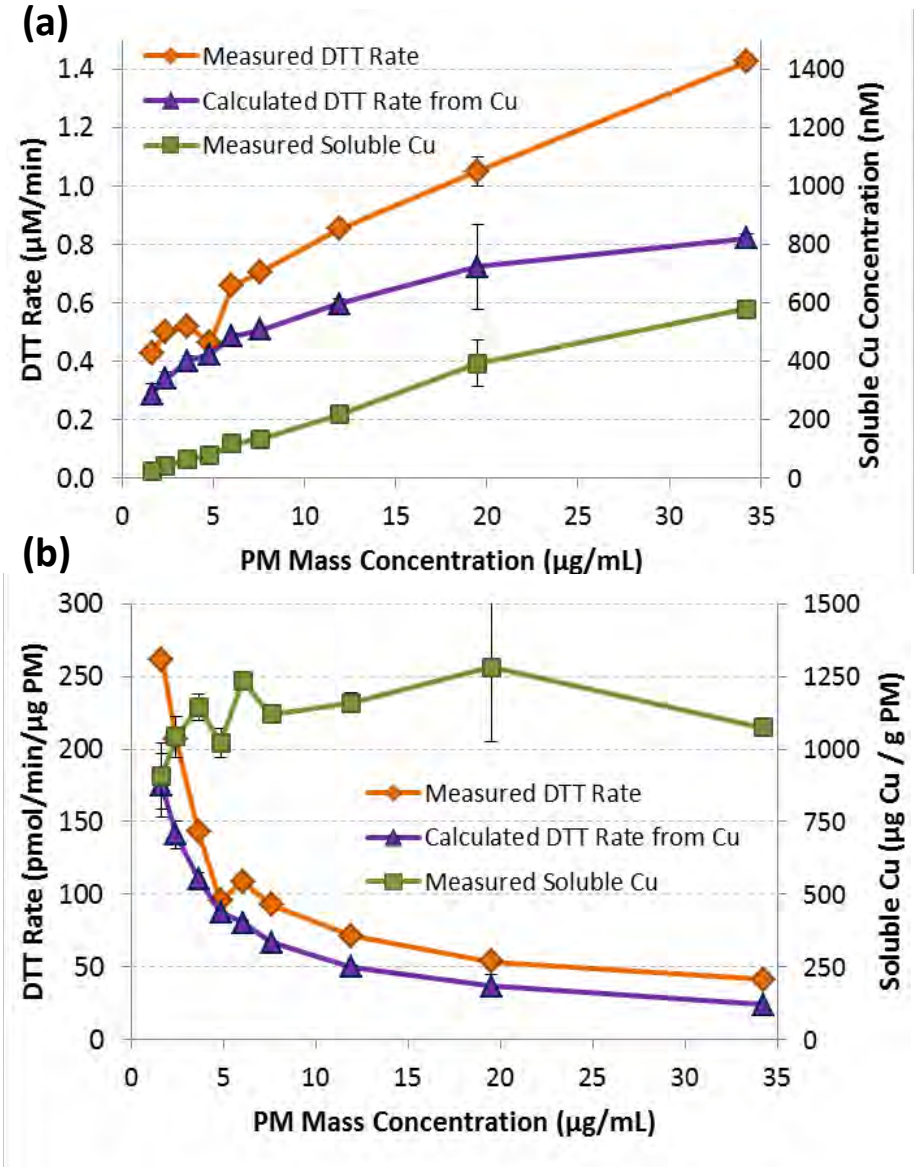

To investigate this mass dependence more closely, we next focus on one sample, C12, that we studied with the greatest number of different mass concentrations. Figure 16 shows the measured DTT response, the calculated DTT response from Cu, and the measured concentration of soluble Cu in each sample in both raw (Figure 16a) and mass-normalized units (4b). All samples are from the same PM filter, with the only difference being the size of the filter piece used. As expected, the soluble Cu concentration varies linearly with the concentration of PM added to the vial (Figure 16a), thus the mass-normalized Cu concentration (µg Cu per g of PM) is independent of the concentration of PM added to the assay within error (Figure 16b). The calculated DTT rate from Cu accounts for most of the measured DTT response, and behaves like the measured DTT response in both units. The measured mass-normalized DTT rate from sample C12 varies between 260 and 40 pmols DTT per minute per µg PM, decreasing with increasing concentration of PM added to the assay. The fact that the soluble Cu concentration (in nM) in each sample extract is linearly proportional to the PM mass concentration (Figure 16a) indicates the mass-dependent DTT result in Figure 16b is not an artifact of PM extraction or an effect of solubility. Additionally, the fact that the measured DTT response follows near identical behavior to the calculated DTT response from Cu, and is similar to Figure 13, indicates that the non-linear Cu concentration-response is driving the result.

While these results indicate a potentially significant artifact in the DTT assay, it is important to note the mass-normalized DTT response will be unbiased (i.e., independent of PM mass concentration) in some cases. For example, samples with low Cu and Mn contents, where most DTT response is attributable to species that have a linear concentration-response should be relatively unbiased. Thus diesel PM samples, or laboratory-generated samples of secondary organic aerosol from organic precursors, should have low amounts of Cu and Mn and thus may produce a robust mass-normalized DTT response. Additionally, samples that were studied near the DTT target concentration of 10 µg PM per mL (discussed below) will show less bias, especially if Cu concentrations are moderate, as we observed in a different ambient PM sample set (Charrier et al. 2015).

Correction of the Mass-Normalized DTT Response

Comparing DTT responses among samples requires a robust mass-normalized DTT result. Because the mass-normalized response is a function of mass, meaningfully comparing rates requires either that researchers measure the DTT response at one standard PM mass concentration for all samples, or that a technique be developed to calculate DTT responses at a standard mass concentration. This mass concentration must be constant for all studies in order to compare DTT data. We propose a standard value of 10 µg of PM per mL of DTT solution, since this is within the range typically used and it provides an adequate DTT response for typical ambient PM.

One way to get a robust mass-normalized DTT response is for the community to measure all samples at a mass concentration of 10 µg per mL. However, this is often impractical, as it would require a consistent PM mass in all DTT extracts regardless of the wide variety of PM collection methodologies. However, if possible to add 10 µg of PM to each DTT assay, then this method would theoretically be the most accurate, as it would not require a correction

calculation. However, significant post sample preparation might be necessary to add a specific mass of PM to the DTT assay, which might affect the results. For example, the removal of PM from sampling substrates can introduce artifacts, such as the loss of semi-volatile quinones during evaporation or drying steps. For these reasons, post-sample processing to add 10 µg per mL to the DTT assay may introduce other significant errors, which would need to be examined.

We thus consider two alternate methods for determining the expected DTT response for samples at 10 µg per mL. The first, the "interpolation" method, requires measuring the DTT response at multiple PM mass concentrations and extrapolating the DTT response to a PM concentration of 10 µg per mL. The second method, the "calculation" method, requires measuring concentrations of DTT-active species in each sample and using concentration-response curves to calculate their dependence on PM mass concentration. The first of these, the "interpolation" method, has the advantage of not requiring chemical analysis, although it requires running each sample at multiple mass concentrations, ideally in a range around 10 µg per mL. We then assume a linear relationship between the raw DTT response (in µM DTT per minute) and the mass concentration of PM and use this line to estimate the rate at 10 µg/mL of PM. As shown in Figure 17 for the eight variable mass samples, there is generally a relatively linear relationship between measured DTT response (µM per minute) and the concentration of PM added to the assay. However, the results will actually follow a curve similar to the total DTT response in Figure 13a, where the magnitude of curvature will depend on the Cu and Mn contents of the PM. This non-linear relationship is subtle but apparent in sample C12 (Figure 17a) where the measured DTT response does not fit the linear regression, and the corrected DTT response at 10 µg per mL is lower than expected from the samples that are closest in concentration. If measured DTT responses surround 10 µg per mL, then the corrected DTT response is interpolated, and should contain less error, while if the measured DTT responses do not encompass 10 µg per mL the corrected DTT response is extrapolated and may contain more error. For samples that allow measurement of DTT response above and below 10 µg per mL, as in sample C12, a corrected result using the linear interpolation of the points immediately surrounding 10 µg per mL will provide the most accurate result.

A second potential source of error in the "interpolation" method is illustrated in samples C19, F17, and F28 (Figures 5b, 5f, and 5g respectively), where the measured DTT responses do not encompass 10 µg per mL. A corrected DTT response extrapolated far outside the measured DTT response can increase the uncertainty in the corrected DTT response, as the divergence from linear will become

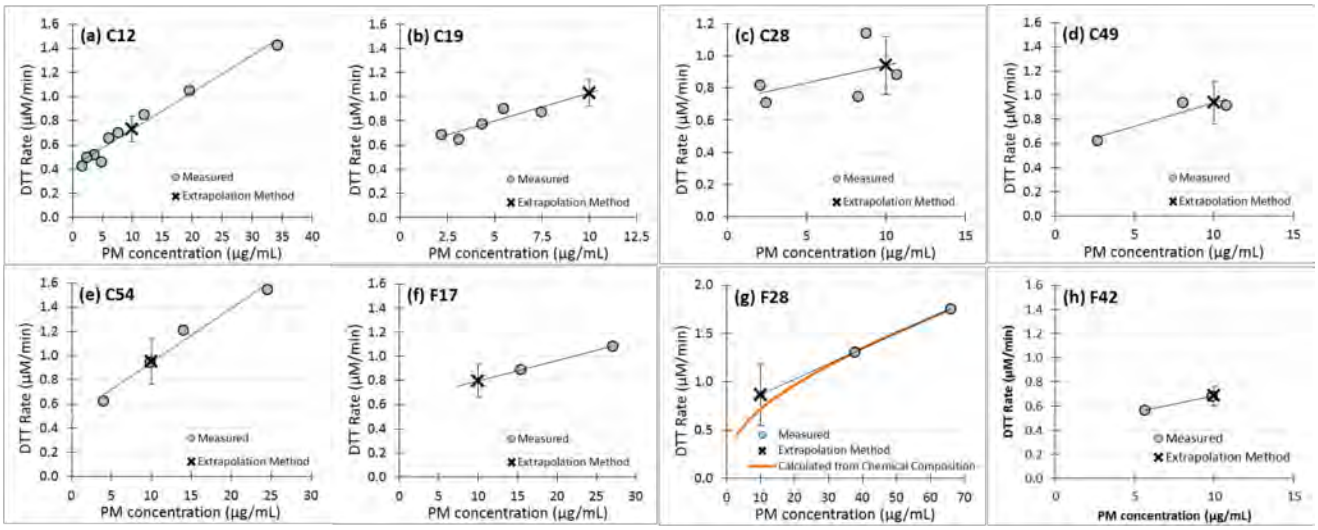

Figure 17. Measured rate of DTT response (blue circles) and the corrected rate determined at 10 µg PM per mL using the "interpolation" method (black x) for each PM sample. The black line represents the linear regression fit to the measured DTT response, which was used to interpolate (or extrapolate) the DTT response to a PM concentration of 10 µg per mL. The orange line in panel (g) represents the calculated DTT response based on the chemical composition of the sample measured at 65.9 µg PM per mL DTT solution.

increasingly large. This is illustrated in Figure 17g, where the "interpolation" method assumes a linear response (black X), while the calculated DTT response based on the chemical composition of the sample (based on the composition of the sample at 65.9 ug PM per mL DTT solution) shows a curved result (orange line). Thus, the "interpolation" method in this sample would likely overestimate the corrected mass-normalized DTT response. On the other hand, extrapolating from very low masses to 10 µg/mL could lead to an overestimate of the DTT response if the sample has significant curvature. Thus, while the "interpolation" method can produce accurate results when DTT measurements closely surround the 10 µg per mL target and are interpolated over small PM mass differences, accuracy cannot be assured in other cases.

The second method, "calculation", requires measuring the DTT response at only one PM mass concentration (preferably near 10 µg per mL), but necessitates chemically characterizing the DTT-active components in the sample at this concentration. The concentration of each DTT-active chemical component in the PM extract is then assumed to vary linearly with the PM mass added to the vial, allowing calculation of the composition at 10 µg per mL. These normalized concentrations are next used in the DTT concentration-response equations (Charrier and Anastasio (2012b) and equation 1) to calculate the DTT response at 10 µg per mL. To achieve accurate results, the concentrations of soluble Cu and Mn must be measured at a minimum in order to account for their non-linear concentration-response curves. All other known species exhibit linear concentration-response curves, so the DTT responses from these species are assumed to be proportional to PM mass concentration. Similarly, we assume that the

concentration-response curves for the unknown species are linear. However, some of these responses for unknown DTT-active species might be non-linear, which would lead to errors in calculation. Therefore, samples with a large contribution from unknown species may require more analysis to ensure accurate normalization. The "calculation" method has the advantage over the "interpolation" method that a wider variety of PM masses could be used in the DTT assay without sacrificing accuracy, because the "calculation" method is able to account for the curve in DTT response as a function of PM concentration (e.g., Figure 17g). However, this method relies on multiple measurements of chemical composition, resulting in larger errors for the calculated mass-normalized DTT result at 10 µg/mL.

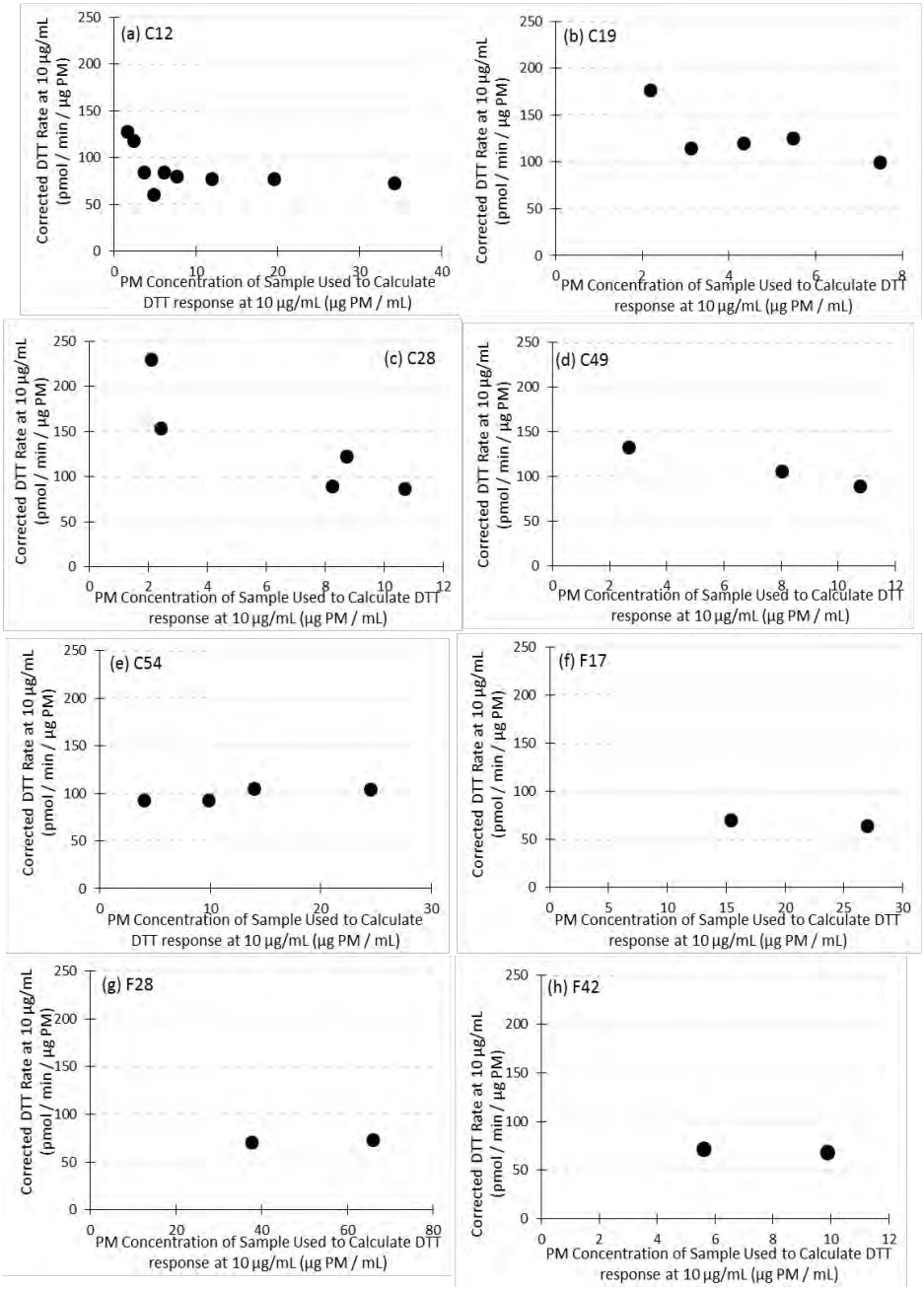

Figure 18. Corrected mass-normalized DTT response using the "calculated" method as a function of starting PM mass concentration.

Using the "calculation" method, for a given sample, any concentration of PM mass used in the assay should result in the same corrected mass-normalized DTT response. To test this, we calculated the corrected mass-normalized DTT result for each measured DTT response at the different concentrations of PM mass used for a given sample. As shown in Figure 18, the "calculated" method gives a relatively consistent corrected mass-normalized DTT response, independent of the starting concentration of PM used for the calculation. The exception is for very low PM mass concentrations, which appear to consistently diverge from the results of the other masses (Figures 6 a, b, c, and d). Based on this result it appears that the "calculation" method cannot be used for samples measured with a PM mass concentration below approximately 4 µg PM per mL.

Comparisons of the two Correction Methods

In Figure 19 we compare the corrected mass-normalized DTT results (using both correction methods) to the measured DTT data for each sample. The two methods provide very similar corrected mass-normalized DTT responses for samples that do not extrapolate far beyond the measured data (i.e., Figure 19 excluding f and g). Under these conditions both methods appear to provide a similar level of accuracy. The results begin to diverge for samples F17 and F28 (Figures 7 f and g), where the corrected results are extrapolated far from the measured values. For samples F17 and F28, the "calculation" method result is more accurate than the "interpolation" method, because the "calculation" method is able to account for the curvature in the DTT response as a function of PM concentration (e.g., Figures 1 and 5a).

Figure 19. Corrected mass-normalized DTT rate for each sample determined using two methods, compared to the measured DTT rate.

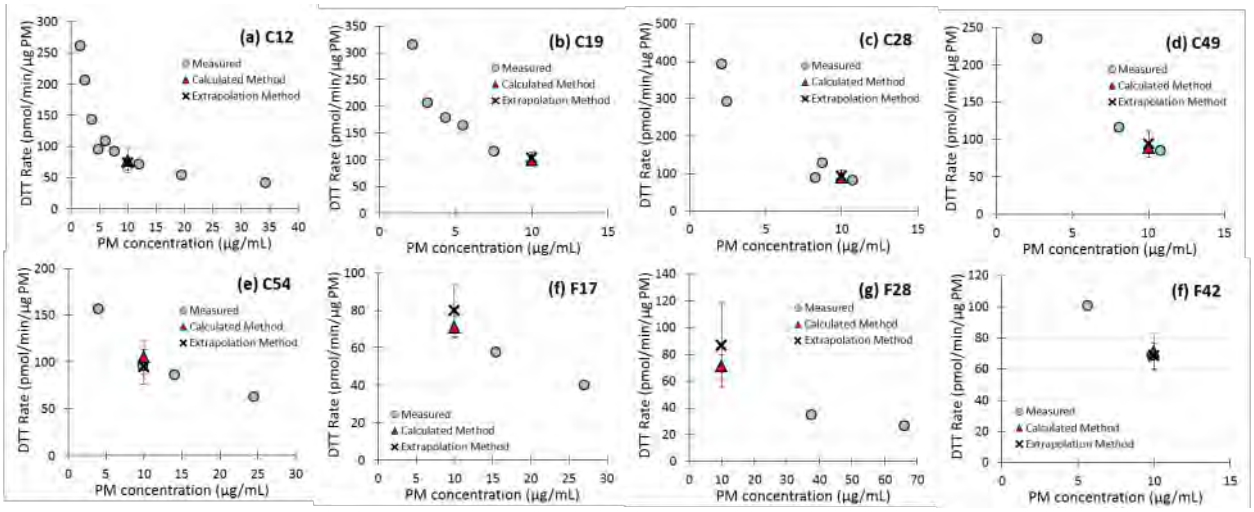

This illustrates one of the main drawbacks of the "interpolation" method: that accuracy cannot be assured if results are extrapolated outside of measured values.

Issues of Non-Linear Responses in Other DTT Applications and Other Assays

There are multiple adaptions of the DTT assay for high-throughput, on-line analyses of ambient PM (Fang et al. 2015; Koehler et al. 2014; Sameenoi et al. 2012; Sameenoi et al. 2013). These DTT assay adaptions are likely susceptible to the same artifact in the mass-normalized response that we observe here, because this artifact is directly tied to the non-linear concentration-response curves for Cu and Mn in the DTT assay. The DTT corrections discussed here generally cannot be applied to on-line methodology as currently used. However, given the mass sensitivity of the mass-normalized DTT responses, it is essential to analyze the potential for this artifact to affect on-line analyses. This could be done, for example, using PM that would exhibit the artifact, such as ambient PM with modestly high Cu and Mn concentrations; in contrast, the artifact might not be apparent in many of the dust or diesel PM samples often used to calibrate or validate on-line techniques. Correction of the DTT assay in on-line techniques may be particularly challenging, but is no less important in order to provide an accurate interpretation of oxidative potential from the DTT assay.

Unfortunately, the mass dependence of the "mass-normalized" result in the DTT assay likely also occurs in other assays. Indeed, any assay where an important redox-active species exhibits a non-linear concentration-response curve likely suffers from a similar bias. For example, Cu has non-linear concentration-response curves in assays that measure the generation of hydroxyl radical ($^{\cdot}OH$) (Charrier and Anastasio 2015a; Vidrio et al. 2008) and hydrogen peroxide (HOOH) (Charrier et al. 2014; Shen et al. 2011) in a cell-free surrogate lung fluid. Since Cu is a

major component of both OH and HOOH generation from ambient PM (DiStefano et al. 2009; Richards-Henderson et al. 2015; Shen and Anastasio 2011b; Shen et al. 2011; Shen and Anastasio 2012; Vidrio et al. 2009), the measured rates are likely affected by the PM mass employed, although this has not been examined. Further work is necessary to determine if this bias occurs at PM concentrations typically included in the assays, and to examine whether the methods for correcting DTT data we describe for DTT here can also apply to these other assays.

Conclusions

We have shown that ambient $PM_{2.5}$ samples collected at two different sites in California exhibit bias in the mass-normalized DTT result, which confounds the ability to compare results among samples without correction. This bias is a consequence of the non-linear concentration-response curves of soluble copper and manganese in the DTT assay. As such, the bias will be most pronounced in samples with a large DTT contribution from copper and/or manganese, such as those used in this work. In samples such as these, which appear to be common in the atmosphere, lower masses used in the DTT assay will result in higher (uncorrected) mass-normalized DTT responses, even for the same samples.

We also present two methods to correct the mass-normalized DTT results: (1) the "interpolation" method, which uses DTT measurements at multiple PM mass concentrations for a given sample to interpolate the DTT response to 10 µg PM per mL, and (2) the "calculation" method, which uses a single measured DTT response, along with the measured Cu and Mn concentrations in the sample extract, to predict the DTT response at 10 µg PM per mL. Either method can be used to correct the mass-normalized DTT response, within certain parameters. The "interpolation" method is accurate if the DTT response for a given sample is measured over multiple PM concentrations in a relatively narrow window around 10 µg PM per mL. In the second method, "calculation", the DTT response is only measured at one PM mass concentration, but the concentrations of Cu, Mn, and, preferably, other redox-active species are measured in the PM extract. This method is accurate for PM concentrations greater than approximately 4 µg PM per mL of DTT solution, and can be extrapolated over a wider range of PM concentrations. However, neither of these correction methods appears to be usable in the new, high throughput, on-line DTT assays as they are currently run. Further research into the potential effects of the mass concentration bias, and the utility of the correction techniques, must be performed to ensure the integrity of high-throughput on-line DTT data. Additionally, the mass concentration bias observed in the DTT assay likely also occurs in any assay where a major redox-active species has a non-linear concentration-response curve. This probably applies, for example, to cell-free assays that measure specific reactive oxygen species, such as hydroxyl radical and hydrogen peroxide, since Cu has non-linear concentration-response curves in both assays.

Finally, while "mass-normalized" results from the DTT assay (and, likely, other techniques) can suffer from a mass-dependence artifact, this does not impact the ability of the assay to quantitatively determine which redox-active species are responsible for the measured response (e.g., Charrier and Anastasio, 2012; Charrier et al., 2015). However, if non-linear species such as Cu and Mn are important in the response, the relative importance of every redox-active

species in a given PM sample will change as a function of PM mass concentration used in the assay.

IV.B.1

III.D. Dithiothreitol (DTT) Redox-Activity of Particulate Matter from Field Campaigns

Average Metal and Quinone Concentrations. As discussed earlier, the mass concentrations of metals and quinones at Claremont and Fresno are highly variable in time, especially at the latter site. Figure A shows the average values for the metals and quinones at our two sites compared to averages reported from past work in the U.S. In general, our concentrations are similar to previous values, especially compared to the values from larger urban area. Since copper, manganese, and phenanthraquinone (PQN) are expected to be major contributors to the DTT response (Charrier and Anastasio 2012a), we next look in more detail at their values. Our Mn values are on the low end of previously reported ranges, while our PQN values span the range, with higher values in Fresno (Figure A). For Cu, the average (± 1 σ) concentrations at Claremont (24.4 ± 12.8 ng m^{-3}) and Fresno (25.1 ± 19.6 ng m^{-3}) are about 30% lower than the average measured previously in Los Angeles during summer (38.2 ng m^{-3}) (Verma et al. 2009). These values are approximately an order of magnitude higher than those reported for other, much smaller, urban areas, where copper concentrations range from 1 – 2 ng m^{-3} (Figure A) (Connell et al. 2006; Vidrio et al. 2009). This difference is probably explained by variations in traffic density, as a major source of fine particulate copper appears to be brake wear.

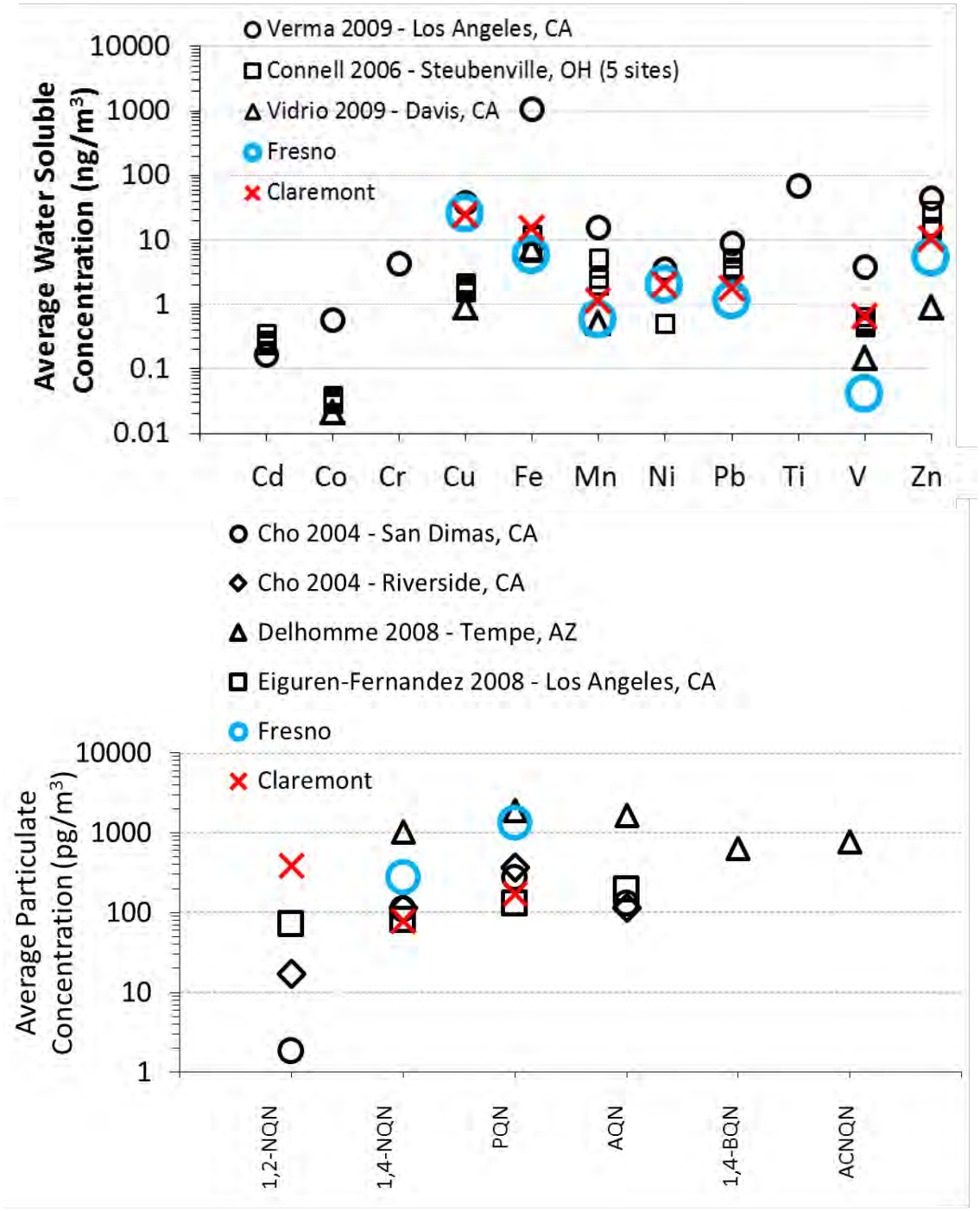

Figure A. Average soluble metals (panel A) and quinone (panel B) concentrations in our Claremont and Fresno samples compared to water-soluble metals and total quinone concentrations in $PM_{2.5}$ from a number of other studies in urban and suburban areas of the U.S. (Cho et al. 2004; Connell et al. 2006; Delhomme et al. 2008; Eiguren-Fernandez et al. 2010; Verma et al. 2009; Vidrio et al. 2009). Each point represents the average value for a given location in each study. 1,2-NQN levels for Fresno samples were always below the detection limit, which ranged from 200 – 870 pg m^{-3}.

However, because our Cu concentrations are quite high, we were interested whether the high-volume sampler might be a source of Cu contamination in our samples. To test whether this

could occur, we collected samples at Fresno in summer 2013 under three sampler configurations: (a) Base case, where the exhaust from the sampler was not controlled (which was the condition we used for our Claremont and Fresno sampling), (b) Low case, where the exhaust was routed away from the sampler (through approximately 10 feet of tubing), and (c) High case, where the exhaust was piped directly into the sampler intake. Each case was sampled for one day, with 3 separate periods for morning, afternoon, and overnight, to mimic our field sampling. Figure B shows that the copper concentrations in the Base and Low conditions are very low, a few ng m^{-3}, while the High case has very high concentrations, approximately 60 – 100 ng m^{-3}. These results indicate that the Hi-Vol sampler exhaust can be a source of particulate copper, but also suggest that under typical operating conditions sample contamination is minor. However, given the importance of Cu in ROS generation (Charrier and Anastasio 2012a; Charrier et al. 2014; Charrier and Anastasio 2015b), this is an issue that should be examined in more detail.

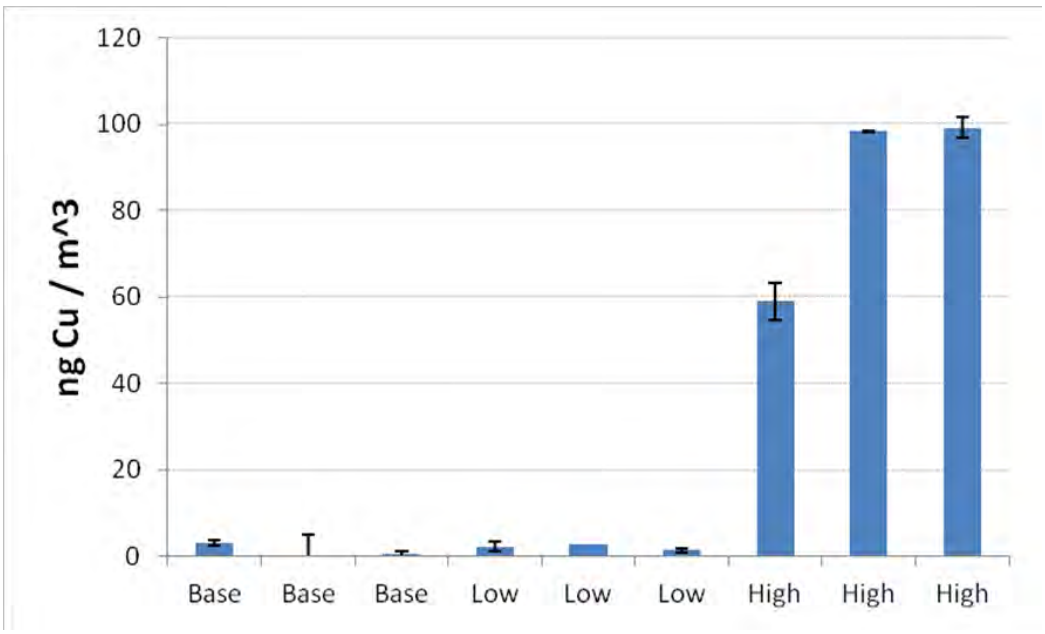

Figure B. Copper concentrations in samples collected to test whether the sampler is a potential source of contamination. Under each condition (Base, Low, High) we collected a sample during morning, afternoon, and overnight.

Finally, we were curious why the Base case samples in Fresno during the summer 2013 sampling had much lower Cu concentrations than the winter 2013 samples we collected in Fresno. Examining the ARB data from the Fresno 1st Street site (http://www.arb.ca.gov/adam/) shows that Cu has a pronounced seasonal cycle, with minimum values during the summer of a few ng m^{-3} and maximum values in the winter that are highly variable and peak at approximately 30 ng m^{-3} (Figure B). Overlaid on this plot are the values from our Fresno sampling, which also show high variability but generally good agreement with the 1st Street

concentrations. This is additional evidence that our Fresno copper concentrations are not significantly affected by contamination from the sampler. There is no ARB Cu data for Claremont so we cannot do a comparison for this site.

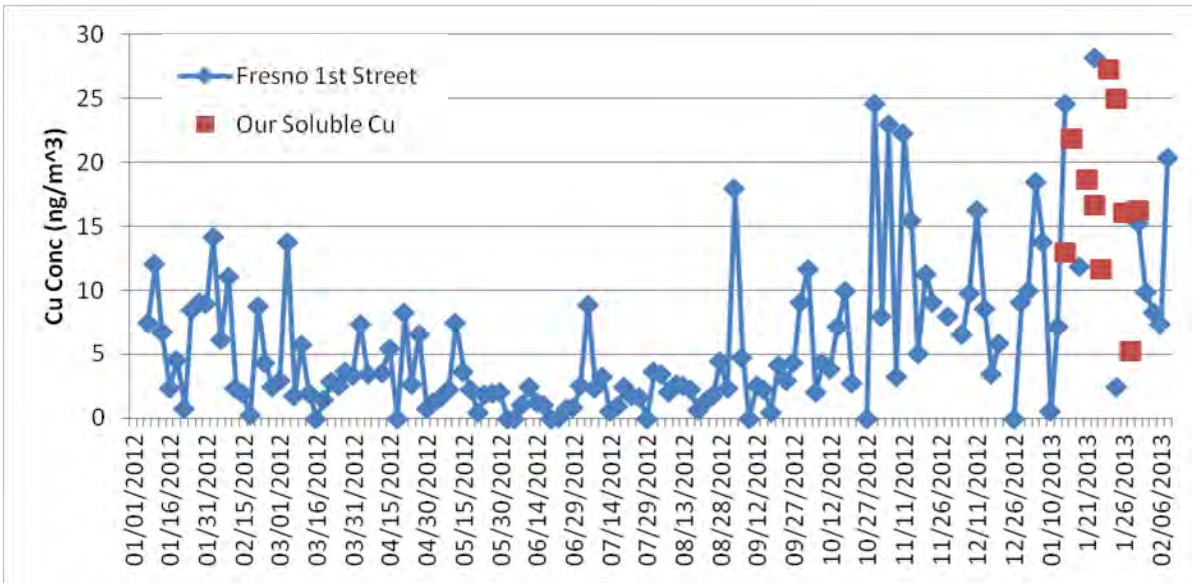

Figure C. Copper concentrations in ambient samples collected by ARB at the 1st Street site in Fresno (blue diamonds) compared to our Fresno samples (red squares).

3.2 Correcting Mass-Normalized DTT Data. During this project we discovered that there is a

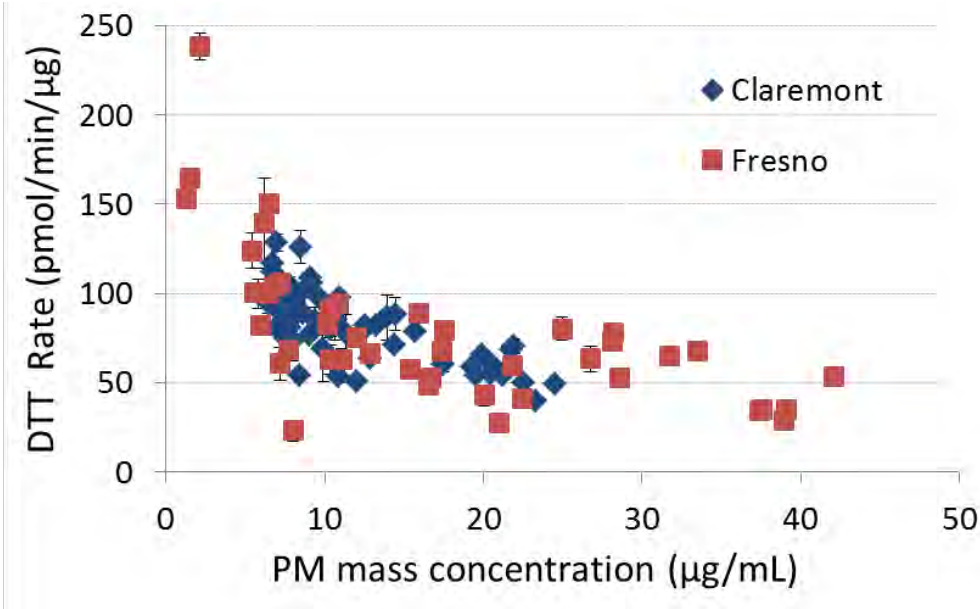

Figure D. Mass-normalized rates of DTT loss as a function of the PM mass concentration used in each extract solution. Each symbol represents a different sample.

bias in mass-normalized DTT data for samples where Cu and/or Mn contribute significantly to the DTT response, as we discuss in section III.C. Figure D shows this problem for our Claremont and Fresno samples: the mass-normalized rates generally decrease with increasing PM mass concentration used in the DTT extract solution. This is a result of the non-linear concentration-response curve for Cu (and Mn), where the rate of DTT loss approaches a plateau at higher Cu (and Mn) concentrations (Charrier and Anastasio, 2012). To correct the data we employed the "calculation" method described in section III.C, which normalizes the data to the DTT response expected for the same PM mass concentration for all samples (10 µg mL^{-1}). This correction removes the artifact of mass-dependence of the DTT response and, in doing so, reduces the variability of the DTT response between different samples (Figure E): (1) the mass-normalized rate is decreased in samples that had an artificially high response because of a low PM mass concentration in the extract, while (2) the rate is increased in samples that had an artificially low response because of a high PM mass concentration. While the PM extract mass in our samples has a large impact on the (uncorrected) mass-normalized rate of DTT loss, it is unclear how important this artifact has been in past studies with DTT.

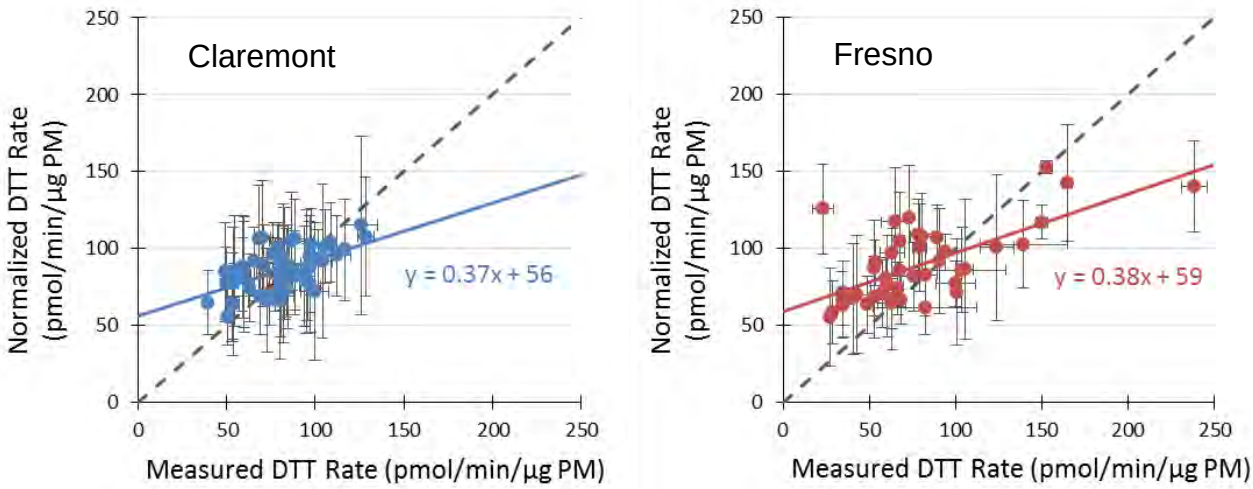

Figure E. Comparison of the mass-normalized rates of DTT loss in the particle extracts before and after correction to a constant PM mass concentration in the extract. The "measured" rate is the value determined in the DTT extract (divided by the extract PM mass concentration), while the "normalized" rate is corrected to a standard extract PM mass concentration of 10 µg mL^{-1}.

III.E. HULIS separation method development

III.E.1 Introduction

A direct measurement of hydroxyl radical in aqueous solutions is difficult due to its low concentration, short lifetime and chemical and physical similarity to the aqueous solvent. Chemical probes such as benzene (Faust and Allen 1993), nitrobenzene [Zepp et al., 1992], benzoic acid (Jung et al. 2006), and terephthalic acid (Li et al. 2007; Matthews 1980; Saran and Summer 1999); Charbouillot et al.,2011] have been used to detect OH radicals by reacting with it to form hydroxylated products, which in turn are detected using fluorescence (terephthalic acid) or UV absorption (benzene derivatives). Reported detection limits are in a similar range; 50 and 30 nM for terephthalic (Saran and Summer 1999) and benzoic (Shen et al. 2011) acid respectively. Of the hydroxyl radical probes, terephthalic acid has several advantages. Due to its symmetric configuration, OH reaction with terephthalate results in only one ring-preserving product, 2-hydroxyterephthalic acid. Furthermore, 2-hydroxyterephthalic acid is strongly fluorescent (Armstrong et al. 1963), and fluorescence is a more specific assay than UV absorption. This offers the possibility that the terephthalic acid assay may be used without a separation step under many circumstances. Avoiding a separation step facilitates more detection options; much more sensitive spectrometers with more sample size options are available for stand-alone fluorescence detection than for High Performance Liquid Chromatography (HPLC)-fluorescence.

While the TA method offers a selective and highly sensitive technique, it is subject to interference from other species with native fluorescence in the same wavelength range as HTA. Further, it is sensitive to the presence of compounds that absorb, at both its absorption and fluorescence wavelengths. Most compounds common in atmospheric aerosol and surface waters, including inorganic salts and acids, water and most organics do not fluoresce or absorb at the wavelengths of interest here. Compounds such as soot and some oxygenated organics may have some fluorescence and or absorption activity, but at typical concentrations in ambient aerosol samples they are too small to measurably to interfere. Biomass-burning aerosol, however is a notable exception as it contains a large fraction of complex organics and black carbon (Andreae and Merlet 2001; Cachier et al. 1995). Strong fluorescence of both atmospheric and surface water organic carbon such as fulvic and humic acids (FA and HA) has been reported by several groups (Duarte et al. 2004; Krivacsy et al. 2000; Nakajima et al. 2008), thus FA and HA may also interfere. Fluorescence regions include those that specifically interfere with the HTA assay, making use of TA as a probe difficult when significant quantities of fluorescent-complex water-soluble organic compound (WSOC) material is present in the samples. Pullin and co-workers (Mobed et al. 1996; Pullin and Cabaniss 1995) examined the pH-dependent synchronous fluorescence spectra of six standard humic substances and showed that their spectra are strongly pH dependent; the fluorescence intensity of humic substances decreases with decreasing pH decreases over the range 3-11 by a factor of 3 or more at most wavelengths. Similar but weaker trends have been observed for fresh water dissolved organic matter from various locations in UK (Spencer et al. 2007). As a result, samples with moderate to high concentrations of complex organics may require additional steps to quantify OH, especially if the samples are at higher pH; simply lowering the pH can cause precipitation of the HULIS (see below).

Varga et al. (2001) developed a method to isolate HULIS using a hydrophilic lipophilic balance sorbent material. Similar methods to isolate HULIS in ambient samples based on HLB separations have been reported by several additional studies (Kuang et al. 2015; Lin et al. 2010; Lin and Yu 2011; Varga et al. 2001; Verma et al. 2012). HLB is a reverse phase sorbent for acidic, basic and neutral compounds, consisting of two monomers: hydrophilic N-vinylpyrrolidone and lipophilic divinylbenzene. Biomass burning WSOC, fulvic and humic acids are believed to be comprised of phenolic, hydroxylic, carboxylic, and aliphatic chains, and aromatic rings and polysaccharides (Decesari et al. 2001; Duarte et al. 2005; Havers et al. 1998; Krivácsy et al. 2001; Mayol-Bracero et al. 2002); either as aggregates of smaller molecules or macromolecules (Piccolo and Conte 2000).

While HTA is a much smaller molecule than HULIS, it shares many chemical characteristics, including a contribution from an aromatic ring, and hydroxyl and carboxylic acid functional groups with FA, HA and WSOC/HULIS, presenting challenges for its separation. Nevertheless, by substantially adjusting the eluent system, we are able to develop a straightforward method that successfully separates fulvic and humic acids as well as BBHULIS from HTA with high efficiency.

III.E.2. Specific Methods

(See also Methods Section for additional details)

III.E.2.1 Fluorescence Spectroscopy and quantification of HTA

HTA fluorescence intensity was measured at excitation/emission wavelengths of 320 and 420 nm respectively with a Lumina Fluorescence Spectrometer (Thermo Scientific). HTA calibration curves were prepared in pH 3.5 or 7.4 at HTA concentrations of 50, 100, 500 and 800 nM. A 10^{-3} M Stock solution of HTA in milli-Q water (18MΩ.cm) was prepared using an acid cleaned Teflon bottle which was wrapped in aluminum, and stored in the refrigerator. Calibration of HTA fluorescence was performed prior to each experiment using 5 dilutions. The 1mg/mL HA/FA stock solution was prepared weekly.

The excitation-Emission Matrix (EEM) scan mode was used to elucidate the fluorescence features for HTA, HA/FA and SBBHULIS from ambient samples. EEM scans were performed with 10 nm excitation and emission slit widths, 60nm/s scan speed and 10ms integration time. Excitation spanned about 280 - 500nm, and emission about 300 – 600 nm, with 5 nm intervals.

Analyte recovery analyses of HTA were performed by measuring the fluorescence 800nM of HTA before and after column separation using single-read scan, in which the maximum excitation and emission wavelengths are scanned in a fast and sensitive manner. Analyte recovery/breakthrough analyses of FA, HA and BBHULIS were performed in a similar manner in which their fluorescence was measured at the respective maximum excitation and emission wavelengths before and after column separation.

Biomass Burning HULIS Collection and Extraction

Shortly after collection, the Fresno samples were weighed using a microbalance to determine the aerosol mass concentration. One square inch of the filter was cut using a ceramic blade (to avoid metal contamination) and was extracted with gentle agitation for 2 hours in phosphate buffer (pH 7.4) containing 4 antioxidants at physiologically relevant concentrations: 100 μM uric acid, 100 μM L-glutathione, 200 μM ascorbic acid and 300 μM citrate and 100 mM terephthalic acid. 125μL aliquots of the extraction solution were used in separations. The HLB column was first conditioned with 250μL methanol and then equilibrated with 250 μL Milli-Q water. 125 μL of sample was acidified to a pH 1.34, with sulfuric acid and then loaded on the column. The column was washed with 250 μL water, followed by a 10% methanol:water solution. Final elution steps are described below.

III.E.3. Separation of hydroxy-terephthalate from fulvic acid, humic acid, and biomass burning humic-like substances (HULIS).

Fluorescence characteristics of HTA, HA, FA and SBBHULIS

Sample scanning excitation-emission fluorescence spectra can be found in the literature (Duarte et al. 2004; Mobed et al. 1996; Page et al. 2010; Sierra et al. 2005). Summarizing, the EEM spectrum of HTA is very confined and symmetrical, with a maximum intensity of HTA at $\lambda_{ex}/\lambda_{em}$ of 320nm and 418nm, consistent with a single fluorophore. pH 7.3 EEM spectra of fulvic

Acid have $\lambda_{ex}/\lambda_{em}$ of 340-370 nm and 460-470nm respectively. Humic acid exhibited an even broader spectrum, with 2 peaks at $\lambda_{ex}/\lambda_{em}$ of 360-420nm and 450-460nm and $\lambda_{ex}/\lambda_{em}$ 460nm and 500-540nm respectively. As such, both FA and HA do not directly interfere by absorbing incoming 320 nm photons, however they absorb emitted photons and reduce fluorescence signal. The relatively broad spectra are both consistent with the presence of multiple fluorophores in both fulvic and humic acids. Humic substances have been shown to increase fluorescence with increasing pH. This has been attributed to changes in fluorescent characteristics of phenols and phenolate functional groups. Phenols have two fluorescence maxima and the intensity of the longer wavelength dominates at higher pH (Lakowicz 2013; Mobed et al. 1996). Furthermore, pH influences conformational changes in humic molecules due to a change in functional group interactions with the solvent, leadings to changes in fluorescence (Miano et al. 1988; Mobed et al. 1996). EEM spectra were also collected for $PM_{2.5}$ nighttime samples collected in Fresno containing significant biomass burning HULIS (BBHULIS); an example is shown in Figure 20. This sample was collected in winter during nighttime in Fresno, which has a mass concentration of 40.5 $\mu g/m^3$, and was extracted in SLF. The EEM spectrum of BBHULIS varies somewhat from sample to sample, but it generally resembles that of fulvic acid, but with $\lambda_{ex}/\lambda_{em}$ of 315nm and 415nm, which directly interferes at both the excitation and emission wavelengths of HTA. Thus it is desirable to develop a method to separate both BBHULIS and FA from HTA.

Inference with HTA measurement by HA/FA

To determine how HA/FA interferes with HTA, different concentrations of FA/HA (from 5 to 50 μg/mL) were added to 800nM of HTA and the fluorescence of the mixture was measured by EEM. Both humic and fulvic acid interfere with HTA at concentrations greater than of 10 μg/mL and higher (not shown). As concentrations of FA and HA increase, the fluorescence intensity at $\lambda_{ex}/\lambda_{em}$ of 320 and 420nm decreases. Stronger fluorescence peaks of FA ($\lambda_{ex}/\lambda_{em}$ of ~360/460nm) and HA ($\lambda_{ex}/\lambda_{em}$ of ~ 370/460nm and $\lambda_{ex}/\lambda_{em}$ of ~ 460/520nm) were observed when FA/HA concentrations were above 10 μg/mL. This effect is especially significant for HA. At FA/HA concentrations below 10 μg/mL EEM scans indicate there is some broadening at longer wavelengths, however the maximum $\lambda_{ex}/\lambda_{em}$ of HTA remains unperturbed (Figures S2 and S3).

Figure 20 shows calibration curves constructed using the much more sensitive single $\lambda_{ex}/\lambda_{em}$ mode. Calibrations of HTA by itself (50-800nM) and with added FA (5-50 µg/mL) were performed. Background fluorescence increases as FA is added, resulting in high intercepts and lower slopes, and concentrations of HTA at lower concentrations (50 – 100 nM) are strongly affected. 800 nM HTA is only significantly affected by 50 µg/mL FA, the highest FA concentration tested.

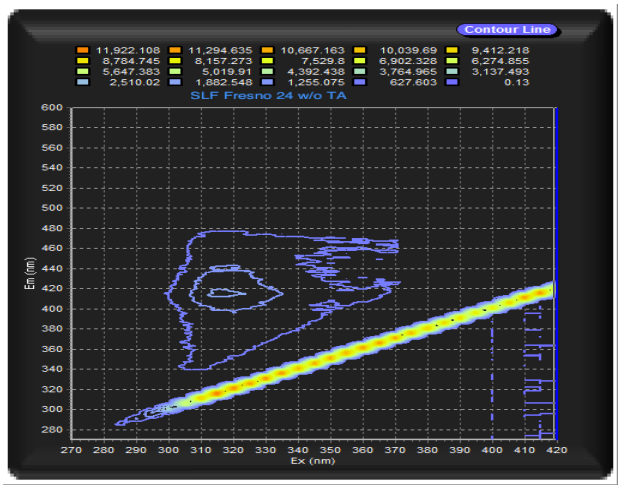

Figure 20. Water-soluble BBHULIS extracted from a nighttime sample (Jan. 22) collected in winter in Fresno, in SLF, with a mass concentration of 40.5µg/m^3.

Separation of HTA from Fulvic and Humic Acids and Biomass Burning Humic-Like Substances (HULIS)

In this study, HLB was chosen to separate HTA from HULIS for several reasons. It is available in small sizes (here we used 10mg sorbent size), suitable for small samples (up to 2mL), it is reasonably inexpensive (~$1.70 per cartridge in 2014), and it is stable over the pH range 0 – 14, offering the capability to use pH to develop effective separation methods. Furthermore, it has been used to successfully isolate atmospheric HULIS. Varga et al. [2001] showed that about 60% of the water soluble organic compounds extracted from aerosol samples collected in a forest could be retained on the HLB Cartridge, and this material contained more than 90% of the fluorescence and 70% of UV absorbance of the total water-soluble organic carbon. HLB columns have been used in similar applications in several other studies (Fan et al. 2012; Krivácsy et al. 2008; Lin et al. 2010) Hydrophilic compounds such as inorganic and small organic acids (oxalate) as well as inorganic ions that typically make up the bulk of ambient aerosols are expected to pass through the cartridge with little or no retention, while larger polar, aromatic ring bearing compounds have higher retention on the cartridge (Varga et al. 2001). Analytes with acid groups are retained on HLB columns when they are fully protonated, after which they can be eluted with methanol (Varga et al. 2001). Practically, compounds have higher retention on the HLB cartridge when they are about pH 2 units below their lowest pK_a, according to the manufacturer (Waters Corporation, 2014). Several groups (Krivácsy et al. 2008; Lin et al. 2010; Varga et al. 2001) have successfully isolated HULIS from atmospheric samples using HLB columns by pre-acidifying to pH 2; the pK_as of Humic acid are ~4 and 9 (Choppin and Kullberg 1978). HTA has pK_as of 3.62, 6.47 and 9.86 (Page et al. 2010).

Varga et al. (2001)'s method to separate HULIS is by loading it onto the HLB column, washing it with water, and then eluting with pure methanol. Due to the chemical similarities of HTA and HULIS, the methanol-water system has limited utility in this separation. By adjusting pH and using a mixture water and methanol in the elution step, we were able to recover 100% of the HTA, and leave most FA/HA on the column, however we were not able to find conditions that resulted in complete separation. Eluting HTA + HA/FA mixture with 90% methanol at pH 1.34 yields the highest recovery of HTA and greatest retention of HA or FA. The eluted samples were evaporated and reconstituted in the original solution.

Application of this procedure to BBHULIS was less successful than it was for FA and HA, thus another eluent system was needed to improve the degree of separation. For the HLB cartridge, the analyte will be strongly adsorbed to the cartridge when is protonated, and would be eluted easier when it is deionized at a pH value higher than the pK_a of the compound of interest, that is, a pH value is higher than the first pK_a of HTA. Since HTA and BBHULIS have distinctive pK_as, we decided to set the pH of eluent system that is high enough to elute HTA while retaining BBHULIS, in this case, we chose pH 4 as the ideal pH as it is higher than the lowest pK_a of HTA (3.62) but does not exceedthe lowest pK_a of humic substances (~4) . Furthermore, when eluting the sample with 90% methanol, it would be very likely that some BBHULIS was eluted as well, therefore, a lower percentage of methanol used in the eluent system is preferred. Combination of lower percentages of methanol of 0, 10 and 20% and phosphate buffer showed lower recovery of HTA, while elution with 70% phosphate buffer at pH4 and 30% methanol showed 100% HTA recovery. Combining both criteria, we arrived at an eluent system of 70% phosphate buffer at pH4 and 30% methanol, which have shown to successfully separate HTA from HULIS (Figure 21).

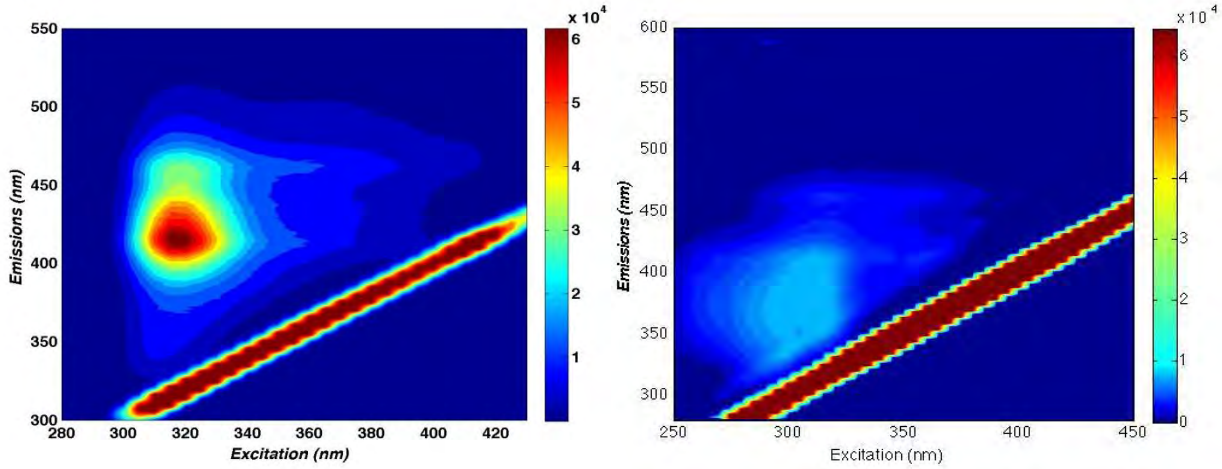

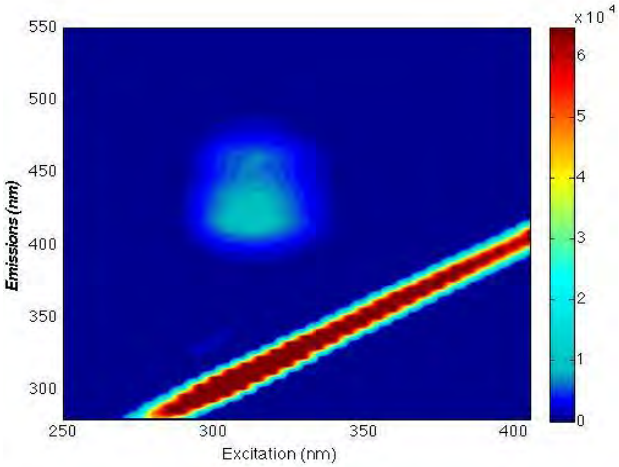

Figure 21. Original aqueous extract of biomass burning aerosol sample without separation (upper left panel); separation of HTA from HULIS using 90% methanol as eluent system, 1:3.3 dilution (upper right panel) and separation of HTA from HULIS using 70% phosphate buffer and 30% methanol as eluent system, 1:6 dilution (lower panel).

When using this eluent system, there was a limitation on the maximum HA/BBHULIS load at which separation is still plausible. As shown in Figure 22, when the concentration of HA was higher than 20 μg/mL, HTA cannot be completely separated from HA when eluted with 70% phosphate buffer at pH 4 and 30% methanol. This suggests that the technique proposed here would not work at higher concentration of HA/HULIS, thus dilution of the sample extract will be needed before applying the separation method.

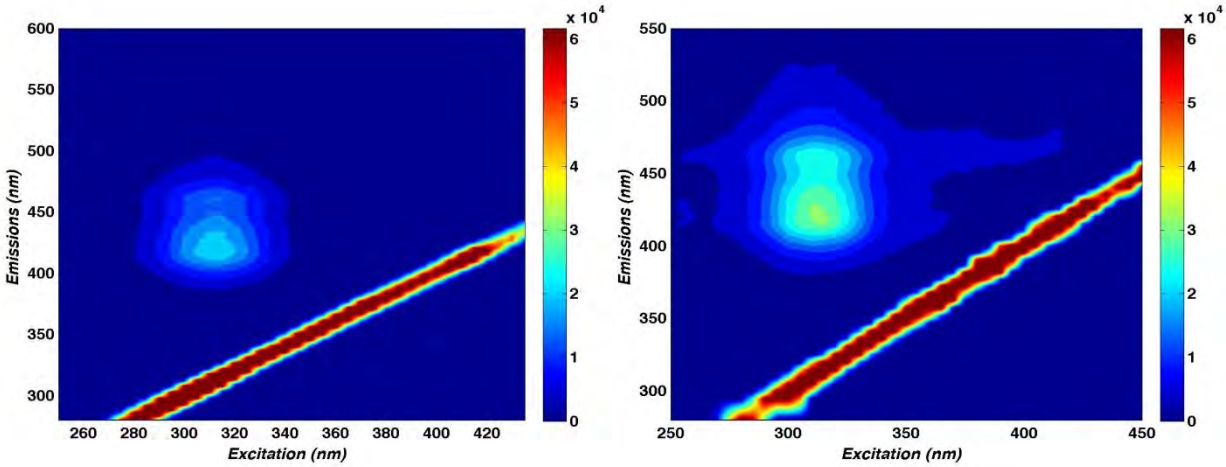

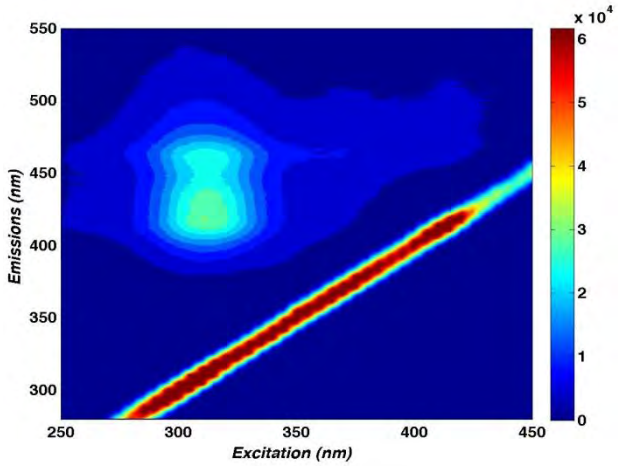

Figure 22. Separation of HTA (800nM) from 20 μg/mL (upper left panel), 40 μg/mL (upper right panel) and 60μg/mL of HA (lower panel) using 70% phosphate buffer at pH 4 and 30% methanol as eluent.

Conclusion

The amount of interference for HTA quantification from fluorescent/absorbing species depends on the concentration of HTA; when HTA is ~50 nM, fulvic and humic acids start to become problematic at about 15 μg/L. Measurement of hydroxyl radicals produced by ambient particulate matter using terephthalic acid as a chemical probe offers great selectivity and sensitivity as well as short analysis time. We provide evidence that the yield of the fluorescent product from the non-fluorescent precursor is about 33% at pH 3.5, indicating that the pH-dependent yields of Matthews et al. (1980) (which have minimal pH dependence) are correct, rather than the yields reported in more recent study (Charbouillot et al. 2011). The presence of a substantial amount of native fluorescence in the same wavelength region as HTA can produce unacceptable interference. To address this issue, a separation method described here using HLB cartridges as the separation media have shown that HTA can be well separated from HA when eluting with 70% phosphate buffer at pH 4 and 30% methanol. This technique was tested to be valid on the separation of HTA from ambient samples containing water-soluble biomass burning HULIS as well as HA/FA derived from soil and aquatic systems.

III.G. References

Andreae, M. O. and Merlet, P. (2001). Emission of trace gases and aerosols from biomass burning. *Glob. Biogeochem. Cycle* 15:955-966.

Armstrong, W. A., Facey, R. A., Grant, D. W. and Humphreys, W. G. (1963). A tissue-equivalent chemical dosimeter sensitive to 1 rad. *Canadian Journal of Chemistry* 41:1575-1577.

Bein, K. J., Zhao, Y. and Wexler, A. S. (2009). Conditional sampling for source-oriented toxicological studies using a single particle mass spectrometer. *Env. Sci. Technol.* 43:9445-9452.

Brun, L. A., Maillet, J., Richarte, J., Herrmann, P. and Remy, J. C. (1998). Relationships between extractable copper, soil properties and copper uptake by wild plants in vineyard soils. *Environ. Pollut.* 102:151-161.

Cachier, H., Liousse, C., Buatmenard, P. and Gaudichet, A. (1995). Particulate content of savanna fire emissions. *Journal Of Atmospheric Chemistry* 22:123-148.

Charrier, J. G. and Anastasio, C. (2011). Impacts of antioxidants on hydroxyl radical production from individual and mixed transition metals in a surrogate lung fluid. *Atmos. Environ.* 45:7555-7562.

Charrier, J. G. and Anastasio, C. (2012a). On dithiothreitol (DTT) as a measure of oxidative potential for ambient particles: Evidence for the importance of soluble transition metals. *Atmos. Chem. Phys.* 12:9321-9333.

Charrier, J. G. and Anastasio, C. (2012b). On dithiothreitol (DTT) as a measure of oxidative potential for ambient particles: evidence for the importance of soluble transition metals. *Atmos. Chem. Phys.* 12:9321-9333.

Charrier, J. G. and Anastasio, C. (2012c). On dithiothreitol (DTT) as a measure of oxidative potential for ambient particles: evidence for the importance of soluble transition metals. *Atmospheric Chemistry and Physics Discussion* 12:8533-8546.

Charrier, J. G., Mcfall, A. S., Richards-Henderson, N. K. and Anastasio, C. (2014). Hydrogen peroxide formation in a surrogate lung fluid by transition metals and quinones present in particulate matter *Env. Sci. Technol.* 48:7010-7017.

Charrier, J. G. and Anastasio, C. (2015a). Rates of hydroxyl radical production from transition netals and quinones in a surrogate lung fluid. *Env. Sci. Technol.* 4:9317-9325.

Charrier, J. G. and Anastasio, C. (2015b). Rates of hydroxyl radical production from transition metals and quinones in a surrogate lung fluid. *Environ. Sci. Technol.* 4:9317-9325.

Charrier, J. G., Richards-Henderson, N. K., Bein, K. J., Mcfall, A. S., Wexler, A. S. and Anastasio, C. (2015). Oxidant production from source-oriented particulate matter - Part 1: Oxidative potential using the dithiothreitol (DTT) assay. *Atmos. Chem. Phys.* Accepted.

Cho, A. K., DiStephano, E., You, Y., Rodriguez, C. E., Schmitz, D. A., Kumagai, Y., Miguel, A. H., Eiguren-Fernandez, A., Kobayashi, T., Avol, E. and Froines, J. R. (2004). Determination of four quinones in diesel exhaust particles, SRM 1649a, and Atmospheric PM2.5. *Aerosol Sci. Technol.* 38:68-81.

Choppin, G. R. and Kullberg, L. (1978). Protonation thermodynamics of humic acid. *Journal of Inorganic and Nuclear Chemistry* 40:651-654.

Chung, M. Y., Lazaro, R. A., Lim, D., Jackson, J., Lyon, J., Rendulic, D. and Hasson, A. S. (2006). Aerosol-borne quinones and reactive oxygen species generation by particulate matter extracts. *Environmental Science & Technology* 40:4880-4886.

Cleland, W. W. (1964). Dithiothreitol, a new protective reagent for SH groups. *Biochemistry* 3:480-482.

Connell, D. P., Winter, S. E., Conrad, V. B., Kim, M. and Crist, K. C. (2006). The Steubenville Comprehensive Air Monitoring Program (SCAMP): Concentrations and solubilities of $PM_{2.5}$ trace elements and their implications for source apportionment and health research. *J Air Waste Manage Assoc* 56:1750-1766.

Daher, N., Ruprecht, A., Invernizzi, G., De Marco, C., Miller-Schulze, J., Heo, J. B., Shafer, M. M., Shelton, B. R., Schauer, J. J. and Sioutas, C. (2012). Characterization, sources and redox activity of fine and coarse particulate matter in Milan, Italy. *Atmos. Environ.* 49:130-141.

Decesari, S., Facchini, M. C., Matta, E., Lettini, F., Mircea, M., Fuzzi, S., Tagliavini, E. and Putaud, J. P. (2001). Chemical features and seasonal variation of fine aerosol water-soluble organic compounds in the Po Valley, Italy. *Atmospheric Environment* 35:3691-3699.

Delhomme, O., Millet, M. and Herckes, P. (2008). Determination of oxygenated polycyclic aromatic hydrocarbons in atmospheric aerosol samples by liquid chromatography-tandem mass spectrometry. *Talanta* 74:703-710.

DiStefano, E., Eiguren-Fernandez, A., Delfino, R. J., Sioutas, C., Froines, J. R. and Cho, A. K. (2009). Determination of metal-based hydroxyl radical generating capacity of ambient and diesel exhaust particles. *Inhal. Tox.* 21:731-738.

Duarte, R., Pio, C. A. and Duarte, A. C. (2004). Synchronous scan and excitation-emission matrix fluorescence spectroscopy of water-soluble organic compounds in atmospheric aerosols. *Journal Of Atmospheric Chemistry* 48:157-171.

Duarte, R. M. B. O., Pio, C. A. and Duarte, A. C. (2005). Spectroscopic study of the water-soluble organic matter isolated from atmospheric aerosols collected under different atmospheric conditions. *Anal. Chim. Acta* 530:7-14.

Dye, J. A., Lehmann, J., McGee, J., Winsett, D. W., Ledbetter, A., Everitt, J., Ghio, A. J. and Costa, D. L. (2001). Acute pulmonary toxicity of particulate matter filter extracts in rats: Coherence with epidemiologic sutides in Utah valley residents. *Environ. Health Perspect.* 109.

Eiguren-Fernandez, A., Shinyashiki, M., Schmitz, D. A., DiStefano, E., Hinds, W., Kumagai, Y., Cho, A. K. and Froines, J. R. (2010). Redox and electrophilic properties of vapor- and particle-phase components of ambient aerosols. *Environ. Res.* 110:207-212.

Fahmy, B. and Cormier, S. A. (2009). Copper oxide nanoparticles induce oxidative stress and cytotoxicity in airway epithelial cells. *Toxicol. Vitro* 23:1365-1371.

Fan, X., Song, J. and Peng, P. a. (2012). Comparison of isolation and quantification methods to measure humic-like substances (HULIS) in atmospheric particles. *Atmospheric Environment* 60:366-374.

Fang, T., Verma, V., Guo, H., King, L. E., Edgerton, E. S. and Weber, R. J. (2015). A semi-automated system for quantifying the oxidative potential of ambient particles in aqueous extracts using the dithiothreitol (DTT) assay: results from the Southeastern Center for Air Pollution and Epidemiology (SCAPE). *Atmos. Meas. Tech.* 8:471-482.

Faust, B. C. and Allen, J. M. (1993). Aqueous-phase photochemical formation of hydroxyl radical in authentic cloudwaters and fogwaters. *Environmental Science & Technology* 27:1221-1224.

Freeman, M. H. and McIntyre, C. R. (2008). Copper-based wood preservatives. *Forest Products Journal* 58:7.

Gasser, M., Riediker, M., Mueller, L., Perrenoud, A., Blank, F., Gehr, P. and Rothen-Rutishauser, B. (2009). Toxic effects of brake wear particles on epithelial lung cells in vitro. *Part. Fibre Toxicol.* 6.

Gerlofs-Nijland, M. E., Dormans, J., Bloemen, H. J. T., Leseman, D., Boere, A. J. F., Kelly, F. J., Mudway, I. S., Jimenez, A. A., Donaldson, K., Guastadisegni, C., Janssen, N. A. H., Brunekreef, B., Sandstrom, T. and Cassee, F. R. (2007). Toxicity of coarse and fine particulate matter from sites with contrasting traffic profiles. *Inhal. Tox.* 19:1055-1069.

Godri, K. J., Harrison, R. M., Evans, T., Baker, T., Dunster, C., Mudway, I. S. and Kelly, F. J. (2011). Increased Oxidative Burden Associated with Traffic Component of Ambient Particulate Matter at Roadside and Urban Background Schools Sites in London. *PLOS One* 6.

Hanna, P. M. and Mason, R. P. (1992). Direct evidence for inhibition of free-radical formation from Cu(I) and hydrogen-peroxide by glutathione and other potential ligands using the EPR spin-trapping technique. *Arc. Biochem. Biophys.* 295:205-213.

Havers, N., Burba, P., Lambert, J. and Klockow, D. (1998). Spectroscopic characterization of humic-like substances in airborne particulate matter. *Journal Of Atmospheric Chemistry* 29:45-54.

Herner, J. D., Green, P. G. and Kleeman, M. J. (2006). Measuring the trace elemental composition of size-resolved airborne particles. *Env. Sci. Technol.* 40:1925-1933.

Hoek, G., Brunekreef, B., Goldbohm, S., Fischer, P. and van den Brandt, P. A. (2002). Association between mortality and indicators of traffic-related air pollution in the Netherlands: a cohort study. *Lancet* 360:1203-1209.

Hoffmann, B., Moebus, S., Mohlenkamp, S., Stang, A., Lehmann, N., Dragano, N., Schmermund, A., Memmesheimer, M., Mann, K., Erbel, R. and Jockel, K. H. (2007). Residential exposure to traffic is associated with coronary atherosclerosis. *Circulation* 116:489-496.

Hu, S., Polidori, A., Arhami, M., Shafer, M. M., Schauer, J. J., Cho, A. and Sioutas, C. (2008). Redox activity and chemical speciation of size fractioned PM in the communities of the Los Angeles-Long Beach harbor. *Atmos. Chem. Phys.* 8:6439-6451.

Hulskotte, J. H. J., van der Gon, H., Visschedijk, A. H. and Schaap, M. (2007). Brake wear from vehicles as an important source of diffuse copper pollution. *Water Sci. Technol.* 56:223-231.

Jing, X., Park, J. H., Peters, T. M. and Thorne, P. S. (2015). Toxicity of copper oxide nanoparticles in lung epithelial cells exposed to air-liquid interface compared with in vivo assessment. *Toxicol. Vitro* 29:502-511.

Jung, H., Guo, B., Anastasio, C. and Kennedy, I. M. (2006). Quantitative measurements of the generation of hydroxyl radicals by soot particles in a surrogate lung fluid. *Atmos. Environ.* 40:1043-1052.

Karlsson, H. L., Cronholm, P., Hedberg, Y., Tornberg, M., De Battice, L., Svedhem, S. and Wallirider, I. O. (2013). Cell membrane damage and protein interaction induced by copper containing nanoparticles - Importance of metal release process. *Toxicology* 313:59-69.

Koehler, K., Shapiro, J., Sameenoi, Y., Henry, C. S. and Volckens, J. (2014). Laboratory evaluation of a microfluidic electrochemical sensor for aerosol oxidative load. *Aerosol Sci. Technol.* 48:489-497.

Krivacsy, Z., Kiss, G., Varga, B., Galambos, I., Sarvari, Z., Gelencser, A., Molnar, A., Fuzzi, S., Facchini, M. C., Zappoli, S., Andracchio, A., Alsberg, T., Hansson, H. C. and Persson, L. (2000). Study of humic-like substances in fog and interstitial aerosol by size-exclusion chromatography and capillary electrophoresis. *Atmospheric Environment* 34:4273-4281.

Krivácsy, Z., Gelencsér, A., Kiss, G., Mészáros, E., Molnár, Á., Hoffer, A., Mészáros, T., Sárvári, Z., Temesi, D. and Varga, B. (2001). Study on the chemical character of water soluble organic compounds in fine atmospheric aerosol at the Jungfraujoch. *Journal of Atmospheric Chemistry* 39:235-259.

Krivácsy, Z., Kiss, G., Ceburnis, D., Jennings, G., Maenhaut, W., Salma, I. and Shooter, D. (2008). Study of water-soluble atmospheric humic matter in urban and marine environments. *Atmospheric Research* 87:1-12.

Kuang, B. Y., Lin, P., Huang, X. H. H. and Yu, J. Z. (2015). Sources of humic-like substances in the Pearl River Delta, China: positive matrix factorization analysis of PM 2.5 major components and source markers. *Atmospheric Chemistry and Physics* 15:1995-2008.

Lakowicz, J. R. (2013). *Principles of fluorescence spectroscopy*. Springer Science & Business Media.

Li, L. X., Abe, Y., Kanagawa, K., Shoji, T., Mashino, T., Mochizuki, M., Aka, M. T. and Miyata, N. (2007). Iron-chelating agents never suppress Fenton reaction but participate in quenching spin-trapped radicals. *Anal. Chim. Acta* 599:315-319.

Li, Y. B. and Trush, M. A. (1993). Oxidation of hydroquinone by copper - chemical mechanism and biological effects. *Arc. Biochem. Biophys.* 300:346-355.

Lin, P., Huang, X.-F., He, L.-Y. and Yu, J. Z. (2010). Abundance and size distribution of HULIS in ambient aerosols at a rural site in South China. *Journal of Aerosol Science* 41:74-87.

Lin, P. and Yu, J. Z. (2011). Generation of reactive oxygen species mediated by humic-like substances in atmospheric aerosols. *Environmental science & technology* 45:10362-10368.

Lough, G. C., Schauer, J. J., Park, J. S., Shafer, M. M., Deminter, J. T. and Weinstein, J. P. (2005). Emissions of metals associated with motor vehicle roadways. *Env. Sci. Technol.* 39:826-836.

Maestre, P., Lambs, L., Thouvenot, J. P. and Berthon, G. (1992). Copper-ligand interactions and physiological free-radical processes - pH-dependent influence of Cu^{2+} ions on Fe^{2+}-driven OH generation. *Free Radical Research Communications* 15:305-317.

Matthews, R. W. (1980). The radiation-chemistry of the terephthalate dosimeter. *Radiat. Res.* 83:27-41.

Mayol-Bracero, O. L., Guyon, P., Graham, B., Roberts, G., Andreae, M. O., Decesari, S., Facchini, M. C., Fuzzi, S. and Artaxo, P. (2002). Water-soluble organic compounds in biomass burning aerosols over Amazonia 2. Apportionment of the chemical composition and importance of the polyacidic fraction. *Journal of Geophysical Research: Atmospheres (1984–2012)* 107:LBA 59-51-LBA 59-15.

Merkofer, M., Kissner, R., Hider, R. C., Brunk, U. T. and Koppenol, W. H. (2006). Fenton chemistry and iron chelation under physiologically relevant conditions: electrochemistry and kinetics. *Chem. Res. Tox.* 19:1263-1269.

Miano, T., Martin, J. and Sposito, G. (1988). Flourescence Spectroscopy of Humic Substances. *Soil Science Society of America Journal* 52:1016-1019.

Mobed, J. J., Hemmingsen, S. L., Autry, J. L. and McGown, L. B. (1996). Fluorescence characterization of IHSS humic substances: Total luminescence spectra with absorbance correction. *Environmental Science & Technology* 30:3061-3065.

Mulier, B., Rahman, I., Watchorn, T., Donaldson, K., MacNee, W. and Jeffery, P. K. (1998). Hydrogen peroxide-induced epithelial injury: the protective role of intracellular nonprotein thiols (NPSH). *Eur. Resp. J.* 11:384-391.

Nakajima, H., Okada, K., Kuroki, Y., Nakama, Y., Handa, D., Arakaki, T. and Tanahara, A. (2008). Photochemical formation of peroxides and fluorescence characteristics of the water-soluble fraction of bulk aerosols collected in Okinawa, Japan. *Atmospheric Environment* 42:3046-3058.

Ntziachristos, L., Froines, J. R., Cho, A. K. and Sioutas, C. (2007). Relationship between redox activity and chemical speciation of size-fractionated particulate matter. *Part. Fibre Toxicol.* 4.

OEHHA (2008). Appendix D. Individual acute, 8-Hour, and chronic reference exposure level summaries. *http://oehha.ca.gov/air/hot_spots/2008/AppendixD1_final.pdf#page=170*.

Ostro, B., Feng, W.-Y., Broadwin, R., Green, S. and Lipsett, M. (2007). The effects of components of fine particulate air pollution on mortality in California: Results from CALFINE. *Environ. Health Perspect.* 115:13 - 19.

Ostro, B., Hu, J., Goldberg, D., Reynolds, P., Hertz, A., Bernstein, L. and Kleeman, M. J. (2015). Associations of mortality with long-term eposures to fine and ultrafine particles, species and sources: results from the California teachers study cohort. *Environ. Health Perspect.* 117:549-556.

Page, S. E., Arnold, W. A. and McNeill, K. (2010). Terephthalate as a probe for photochemically generated hydroxyl radical. *Journal of Environmental Monitoring* 12:1658-1665.

Pettibone, J., Adamcakova-Dodd, A., Thorne, P., O'Shaughnessy, P., Weydert, J. and Grassian, V. (2008). Inflammatory response of mice following inhalation exposure to iron and copper nanoparticles. *Nanotechnology* 2:189-204.

Piccolo, A. and Conte, P. (2000). Molecular size of humic substances. Supramolecular associations versus macromolecular polymers. *Adv. Environ. Res* 3:508-521.

Pullin, M. J. and Cabaniss, S. E. (1995). Rank analysis of the pH-dependent synchronous fluorescence-spectra of six standard humic substances. *Environmental Science & Technology* 29:1460-1467.

Rice, T., Clarke, R. W., Godleski, J. J., Al-Mutairi, E., Jiang, N., Hauser, R. and Paulauskis, J. (2001). Differential ability of transition metals to induce pulmonary inflammation. *Toxicology and Applied Pharmacology* 177:46-53.

Richards-Henderson, N. K., Charrier, J. G., Bein, K. J., Bau, D., Wexler, A. S. and Anastasio, C. (2014). Oxidant production from source-oriented particulate matter – Part 2: Hydrogen peroxide and hydroxyl radical. *Atmos. Chem. Phys.* Submitted.

Richards-Henderson, N. K., Charrier, J. G., Bein, K. J., Bau, D., Wexler, A. S. and Anastasio, C. (2015). Oxidant production from source-oriented particulate matter – Part 2: Hydrogen peroxide and hydroxyl radical. *Atmos. Chem. Phys.* In Preparation.

Sameenoi, Y., Koehler, K., Shapiro, J., Boonsong, K., Sun, Y., Collett, J., Volckens, J. and Henry, C. S. (2012). Microfluidic electrochemical sensor for on-line monitoring of aerosol oxidative activity. *Journal of American Chemical Society* 134:10562-10568.

Sameenoi, Y., Panymeesamer, P., Supalakorn, N., Koehler, K., Chailapakul, O., Henry, C. S. and Volckens, J. (2013). Microfluidic paper-based analytical device for aerosol oxidative activity. *Env. Sci. Technol.* 47:932-940.

Saran, M. and Summer, K. H. (1999). Assaying for hydroxyl radicals: Hydroxylated terephthalate is a superior fluorescence marker than hydroxylated benzoate. *Free Radic. Res.* 31:429-436.

Shang, Y., Chen, C., Li, Y., Zhao, J. and Zhu, T. (2012). Hydroxyl radical generation mechansim during the redox cycling process of 1,4-naphthoquinone. *Env. Sci. Technol.* 46:2935-2942.

Shen, H. and Anastasio, C. (2011a). Formation of hydroxyl radical from San Joaquin Valley particles extracted in a cell-free surrogate lung fluid. *Atmos. Chem. Phys.* 11.

Shen, H. and Anastasio, C. (2011b). Formation of hydroxyl radical from San Joaquin Valley particles extracted in a cell-free surrogate lung fluid. *Atmos. Chem. Phys.* 11:9671-9682.

Shen, H., Barakat, A. I. and Anastasio, C. (2011). Generation of hydrogen peroxide from San Joaquin Valley particles in a cell-free solution. *Atmos. Chem. Phys.* 11:753-765.

Shen, H. and Anastasio, C. (2012). A comparison of hydroxyl radical and hydrogen peroxide generation in ambient particle extracts and laboratory metal solutions. *Atmos. Environ.* 46:665-668.

Sierra, M. M. D., Giovanela, M., Parlanti, E. and Soriano-Sierra, E. J. (2005). Fluorescence fingerprint of fulvic and humic acids from varied origins as viewed by single-scan and excitation/emission matrix techniques. *Chemosphere* 58:715-733.

Spencer, R. G. M., Bolton, L. and Baker, A. (2007). Freeze/thaw and pH effects on freshwater dissolved organic matter fluorescence and absorbance properties from a number of UK locations. *Water Res.* 41:2941-2950.

Varga, B., Kiss, G., Ganszky, I., Gelencser, A. and Krivacsy, Z. (2001). Isolation of water-soluble organic matter from atmospheric aerosol. *Talanta* 55:561-572.

Verma, V., Ning, Z., Cho, A. K., Schauer, J. J., Shafer, M. M. and Sioutas, C. (2009). Redox activity of urban quasi-ultrafine particles from primary and secondary sources. *Atmos. Environ.* 43:6360-6368.

Verma, V., Rico-Martinez, R., Kotra, N., King, L., Liu, J. M., Snell, T. W. and Weber, R. J. (2012). Contribution of Water-Soluble and Insoluble Components and Their Hydrophobic/Hydrophilic Subfractions to the Reactive Oxygen Species-Generating Potential of Fine Ambient Aerosols. *Environmental Science & Technology* 46:11384-11392.

Vidrio, E., Jung, H. and Anastasio, C. (2008). Generation of hydroxyl radicals from dissolved transition metals in surrogate lung fluid solutions. *Atmos. Environ.* 42 4369-4379.

Vidrio, E., Phuah, C. H., Dillner, A. M. and Anastasio, C. (2009). Generation of hydroxyl radicals from ambient fine particles in a surrogate lung fluid solution. *Environ. Sci. Technol.* 43:922-927.

Wang, Y., Arellanes, C. and Paulson, S. E. (2012). Hydrogen peroxide associated with ambient fine-mode, diesel, and biodiesel aerosol particles in Southern California. *Aerosol Sci. Technol.* 46:394-402.